Title

Pseudosynapsis and Decreased Stringency of Meiotic Repair Pathway Choice on the Hemizygous Sex Chromosome of Caenorhabditis elegans Males

Journal

Genetics, 197(2)

ISSN

0016-6731

Authors

Checchi, Paula M

Lawrence, Katherine S

Van, Mike V

et al.

Publication Date

2014-06-01

DOI

10.1534/genetics.114.164152

Peer reviewed

Pseudosynapsis and Decreased Stringency of Meiotic Repair Pathway Choice on the Hemizygous Sex Chromosome of *Caenorhabditis elegans* Males

Paula M. Checchi,[1] Katherine S. Lawrence, Mike V. Van, Braden J. Larson, and JoAnne Engebrecht[2]
Department of Molecular and Cellular Biology, University of California, Davis, California 95616

ABSTRACT During meiosis, accurate chromosome segregation relies on homology to mediate chromosome pairing, synapsis, and crossover recombination. Crossovers are dependent upon formation and repair of double-strand breaks (DSBs) by homologous recombination (HR). In males of many species, sex chromosomes are largely hemizygous, yet DSBs are induced along nonhomologous regions. Here we analyzed the genetic requirements for meiotic DSB repair on the completely hemizygous X chromosome of *Caenorhabditis elegans* males. Our data reveal that the kinetics of DSB formation, chromosome pairing, and synapsis are tightly linked in the male germ line. Moreover, DSB induction on the X is concomitant with a brief period of pseudosynapsis that may allow X sister chromatids to masquerade as homologs. Consistent with this, neither meiotic kleisins nor the SMC-5/6 complex are essential for DSB repair on the X. Furthermore, early processing of X DSBs is dependent on the CtIP/Sae2 homolog COM-1, suggesting that as with paired chromosomes, HR is the preferred pathway. In contrast, the X chromosome is refractory to feedback mechanisms that ensure crossover formation on autosomes. Surprisingly, neither RAD-54 nor BRC-2 are essential for DSB repair on the X, suggesting that unlike autosomes, the X is competent for repair in the absence of HR. When both RAD-54 and the structure-specific nuclease XPF-1 are abrogated, X DSBs persist, suggesting that single-strand annealing is engaged in the absence of HR. Our findings indicate that alteration in sister chromatid interactions and flexibility in DSB repair pathway choice accommodate hemizygosity on sex chromosomes.

MEIOSIS is essential for the formation of haploid gametes for sexual reproduction. Accurate chromosome segregation during meiosis relies on homology between maternal and paternal homologous chromosomes to drive pairing, synapsis, and crossover (CO) recombination. The presence of differentiated sex chromosomes in the heterogametic sex requires modification of these homology-dependent processes. This is significant as the largely nonhomologous X and Y chromosomes in human males display a higher rate of nondisjunction than autosomes, resulting in infertility and developmental disorders such as Klinefelter and Turner syndromes (Shi *et al.* 2001; Lange *et al.* 2009). It is currently unknown how meiosis is altered to accommodate hemizygous sex chromosomes.

Of critical importance to meiotic chromosome segregation is the formation of double-strand breaks (DSBs) catalyzed by the conserved topoisomerase Spo11 and repair by homologous recombination (HR) to generate crossovers (Keeney *et al.* 1997; Dernburg *et al.* 1998). Spo11-induced DSBs are processed by CtIP/Com1/Sae2, the MRN (Mrell-Rad50-Nbs1) complex and multiple nucleases to facilitate repair by HR (Terasawa *et al.* 2008; Manfrini *et al.* 2010; Zakharyevich *et al.* 2010; Garcia *et al.* 2011). Recent studies in *Caenorhabditis elegans* have revealed that COM-1 and MRE-11 promote HR by inhibiting direct religation of DSBs by nonhomologous end joining (NHEJ) (Lemmens *et al.* 2013; Yin and Smolikove 2013). The importance of inhibiting error-prone pathways during meiosis is also exemplified by studies in *Drosophila*, where multiple barriers to NHEJ have been uncovered by mutational analyses (Joyce *et al.* 2012). In mouse oocytes, an error-prone single-strand annealing (SSA) pathway can process extra-chromosomal DNA. SSA requires only small stretches of homology within a single DNA duplex and results in deletions (Fiorenza *et al.* 2001); however, the prevalence of this pathway in meiosis has not been investigated.

doi: 10.1534/genetics.114.164152
Manuscript received February 18, 2014; accepted for publication March 13, 2014
Supporting information is available online at http://www.genetics.org/lookup/suppl/doi:10.1534/genetics.114.164152/-/DC1.
[1]Present address: Department of Biology, Marist College, Poughkeepsie, NY 12601.
[2]Corresponding author: Department of Molecular and Cellular Biology, One Shields Ave, University of California, Davis, CA 95616. E-mail: jengebrecht@ucdavis.edu

In addition to a bias toward repair through HR, the choice of repair template is also tightly regulated during meiosis. Unlike somatic cells where the sister chromatid is the preferred template, meiotic DSBs are preferentially repaired using the homolog. This homolog bias is imposed through regulation of the meiotic recombination machinery as well as meiosis-specific chromosomal axis components and cohesins (Couteau *et al.* 2004; Niu *et al.* 2005; Niu *et al.* 2009; Kim *et al.* 2010; Ho and Burgess 2011; Hong *et al.* 2013; Shin *et al.* 2013; Yan and McKee 2013). Thus, meiotic prophase events have evolved to drive homologous chromosome interactions to ensure formation of crossovers for proper segregation at the meiosis I division. Nonetheless, studies in *Saccharomyces cerevisiae* and *C. elegans* have revealed that the use of the sister chromatid as a template for DSB repair in meiosis occurs and is important for maintaining genome stability (Bickel *et al.* 2010; Goldfarb and Lichten 2010).

Sex chromosomes of the heterogametic sex are largely nonhomologous and therefore require adaptation of these homology-dependent meiotic processes. Interestingly, even the homologous pseudoautosomal region(s) (PARs) of mammalian sex chromosomes require modification of both chromosome structure and the meiotic recombination machinery to promote crossovers (Kauppi *et al.* 2011). Regardless of the extent of homology, meiotic DSBs are induced along the length of sex chromosomes in male *C. elegans*, mice, and humans (Ashley *et al.* 1995; Moens *et al.* 1997; Sciurano *et al.* 2006; Jaramillo-Lambert and Engebrecht 2010; Checchi and Engebrecht 2011). The hemizygous regions of sex chromosomes subsequently undergo meiotic sex chromosome inactivation (MSCI), which is characterized by elaboration of a specialized heterochromatin domain and transcriptional silencing (Turner 2007). One proposed function of MSCI is to prevent recombination between nonhomologous regions of sex chromosomes (McKee and Handel 1993). While there is no direct evidence in support of this hypothesis, it is likely that the repressive chromatin architecture elaborated during MSCI influences how induced DSBs are repaired, as repair is affected by chromatin environment (Van Attikum and Gasser 2009).

To determine how meiotic DSBs are repaired on hemizygous regions of sex chromosomes, we analyzed repair of SPO-11-induced DSBs on the lone X chromosome of *C. elegans* males. In males, the X chromosome completely lacks a homologous partner, yet meiotic DSBs are induced and repaired efficiently (Jaramillo-Lambert and Engebrecht 2010; Checchi and Engebrecht 2011). Additionally, as with mammals, the X chromosome of *C. elegans* males accumulates repressive chromatin marks and is transcriptionally silenced during meiotic prophase (Kelly *et al.* 2002; Bean *et al.* 2004; Checchi and Engebrecht 2011). Taking advantage of the spatiotemporal organization of the *C. elegans* germ line, high-resolution microscopy, and available mutants, we analyzed the requirement of DSB repair pathways, singly and in combination, as well as chromosomal structural components on repair of meiotic DSBs on the single X chromosome of males. We find that there is a brief period of X chromosome pseudosynapsis (*i.e.*, apparent synapsis that does not necessarily constitute full alignment or contain all components of the synaptonemal complex) that we propose allows X sister chromatids to behave as if they are homologs. Consistent with this, neither meiotic kleisins nor the SMC-5/6 complex, implicated in intersister repair, are required for DSB repair on the X chromosome. Further, unlike on autosomes, in the absence of HR an XPF-1-dependent pathway can repair DSBs on the X, suggesting that error-prone SSA can be engaged to repair DSBs on hemizygous sex chromosomes. We propose that both alteration in sister chromatid interactions and flexibility in repair pathway choice on sex chromosomes accommodate hemizygosity during meiosis.

Materials and Methods

Genetics

Maintenance and genetic analyses of worms were performed using standard procedures (Brenner 1974). *C. elegans* var. Bristol (N2) was used as the wild-type strain. The following mutations were used in this study: LGI, *atm-1(gk186)*, *rad-54 (ok615)*; LGII, *smc-5(ok2421)*, *smc-6(ok3294)*, *xpf-1(ok3039)*; LGIII, *met-2(n4256)*, *unc-32(e189)com-1(t1489)*, *cku-80(ok861)*, *lig-4(ok716)*, *brc-2(tm1086)*; LGIV, *fem-3(e1996)*, *him-8(me4)*, *him-3(e1147)*, *zim-2(tm574)*, *rec-8(ok978)*; LGV, *coh-3(gk112) coh-4(tm1857)*, *fog-2(q71)*; and LGX, *lon-2(e678)*. COSA-1::GFP worms were obtained from Anne Villeneuve (Yokoo *et al.* 2012); the LGV lacO integrant was obtained from Paul Sternberg (Gonzalez-Serricchio and Sternberg 2006); the LacO on X strains was derived from lines from Christian Frokjaer-Jensen and Erik Jorgensen; strains harboring the transgene RPA-1::YFP (*opls263*) were obtained from Michael Hengartner (Stergiou *et al.* 2011) and RPA-1::GFP from Julian Blow (Sonneville *et al.* 2012).

fem-3(e1996) X0 females were generated as described in (Jaramillo-Lambert and Engebrecht 2010). Some nematode strains used in this work were provided by the *Caenorhabditis* Genetics Center, which is funded by the National Institutes of Health National Center for Research Resources (NIH NCRR). All strains were propagated at 20°.

Purification of LacI-His$_6$-GFP

The plasmid used for expressing LacI-His$_6$-GFP was a generous gift from Anna Hines (Darby and Hine 2005). Following induction with 0.5 mM IPTG, *E. coli* were lysed and protein purified using nickel beads (Ni-NTA agarose; Qiagen, Valencia, CA).

Cytological analyses

Immunostaining of germ lines was performed as described (Jaramillo-Lambert *et al.* 2007). The following primary antibodies were purchased and used at the indicated dilutions:

mouse anti-histone H3 dimethyl K4 (1:250) (Millipore, Temecula, CA); rabbit anti-COH-3 (1:10,000), rabbit anti-HIM-8 (1:10,000), rabbit anti-RAD-51 (1:10,000), and rabbit anti-GFP (1:500) (Novus Biologicals, Littleton, CO). Guinea pig anti-HTP-3 (1:500), guinea pig anti-HIM-8 (1:500), and rabbit anti-REC-8 (1:1000) were generous gifts from Abby Dernburg and Josef Loidl, respectively. Rabbit anti-SYP-1 (1:200) and rat anti-RAD-51 (1:100) were generously gifted by Anne Villeneuve. The following secondary antibodies from Life Technologies were all used at 1:500 dilutions: Alexa Fluor 555 goat antirat IgG, Alexa Fluor 488 goat antirat IgG, Alexa Fluor 546 goat antimouse IgG, Alexa Fluor 488 goat antimouse IgG, Alexa Fluor 555 goat antirabbit IgG, Alexa Fluor 488 goat antirabbit IgG, and Alexa Fluor 488 goat anti-guinea pig IgG. Alexa Fluor 647 donkey anti-guinea pig, Alexa Fluor 647 donkey antimouse IgG, and Alexa Fluor 647 donkey antirabbit IgG were used at 1:200 dilutions. DAPI (2 μg/ml; Sigma) was used to counterstain DNA.

LacI-His_6-GFP was added directly to dissected gonads following standard fixation at a concentration of 5–25 ng/μl and incubated overnight at 4°. RPA-1::GFP and RPA-1::YFP fluorescence was directly visualized by dissecting gonads and fixing in 2.5% paraformaldehyde for 1 min. Slides were subsequently incubated on dry ice for at least 5 min followed by freeze crack and immersion in 95% ethanol for 1 min.

Collection of images was performed using an API Delta Vision deconvolution microscope. Images were deconvolved using Applied Precision SoftWoRx image analysis software and subsequently processed and analyzed using Fiji (ImageJA) (Wayne Rasband, NIH). All images shown are projections through data stacks.

Structured illumination microscopy (SIM) analysis was performed using a Nikon N-SIM super-resolution microscope and NIS-Elements 2 image processing software. Images were further processed using ImageJ.

Fluorescent in situ hybridization

Fluorescent in situ hybridization (FISH) was performed as described in Phillips and Dernburg (2006). A fluorescent Cy5-tagged lacO oligonucleotide (5′/5Cy5/CCACATGTG GAATTGTGAGCGGATAACAATTTGTGG-3′) was generated and used to label LacO insertions. Nuclei scored as containing one spot had either a single focus or two adjacent foci whose signals overlapped; nuclei scored as containing two spots had clearly separated signals. Significance was analyzed using Fisher's exact test.

RNA-mediated interference analysis

RNA-mediated interference (RNAi) experiments were performed at 20°, using the feeding method (Timmons *et al.* 2001). L4 larvae were fed RNAi-inducing HT115(DE3) bacteria strains or the same bacteria transformed with the empty feeding vector, L4440. *atm-1* was obtained from a genomic RNAi feeding library (Kamath and Ahringer 2003) and *smc-6* was cloned from N2 genomic DNA into L4440. Cultures were plated onto NGM plates containing 25 μg/ml carbenicillin and 1 mM IPTG and were used within 2 weeks of plating.

Analysis of fragmented chromosomes and progeny inviability

Number of DAPI-stained bodies present in the −1 to −3 diakinesis nuclei of *fem-3(e1996)* X0 and XX worms with indicated RNAi treatment were scored by standard fluorescence microscopy; a minimum of 70 nuclei was examined for each genotype. Significance was analyzed using Fisher's exact test. Percentages of male and inviable progeny were determined from a minimum of eight independent crosses of indicated males to *fog-2(q71)* females. No significant differences were observed using the Student's *t*-test.

Results

Kinetics of chromosome pairing and synapsis are tightly linked with RAD-51 assembly in the male germ line

Meiotic DSBs catalyzed by the conserved topoisomerase Spo11 are essential for crossover formation and successful meiosis. Although Spo11-dependent DSBs are a prerequisite for chromosome pairing and synapsis in many organisms such as yeast and mammals (Giroux *et al.* 1989; Romanienko and Camerini-Otero 2000), these events can be uncoupled by mutational analysis in other species including *Drosophila* and *C. elegans*, as *spo-11* mutants are competent for chromosome pairing and synaptonemal complex (SC) assembly (Dernburg *et al.* 1998; Liu *et al.* 2002). In *C. elegans*, kinetics of meiotic DSB repair are monitored by the appearance and disappearance of immunostained RAD-51 recombinase within the spatiotemporal gradient of the germ line (Colaiacovo *et al.* 2003) (Figure 1A and Supporting Information, Figure S1). While in *C. elegans* hermaphrodites, DSBs peak in abundance in nuclei with fully assembled SCs in early (EP) to mid pachytene (MP) (Colaiacovo *et al.* 2003), RAD-51 foci are more abundant in transition zone (TZ; leptotene/zygotene) in the male germ line (Jaramillo-Lambert and Engebrecht 2010). Interestingly, the male germ line contains more TZ nuclei than in hermaphrodites [53.6 ± 2.0 TZ nuclei/bisected gonad (n = 11) *vs.* 36.1 ± 1.6 TZ nuclei/bisected gonad (n = 9); $P < 0.001$], suggesting that the early peak of RAD-51 foci may reflect alteration of the kinetics of chromosome pairing in the male germ line. To investigate the spatiotemporal relationship between chromosome pairing and the appearance of meiotic DSBs in the *C. elegans* male germ line, we monitored RAD-51 assembly in germ lines containing a LacO insertion on chromosome V (LacO-V), which allowed us to track homolog interactions throughout all stages of meiotic progression using purified LacI-His_6-GFP (Figure 1).

The *C. elegans* male germ line has five pairs of autosomes and one sex chromosome, the X. Although the X lacks a homolog and cannot form a chiasma, all chromosomes

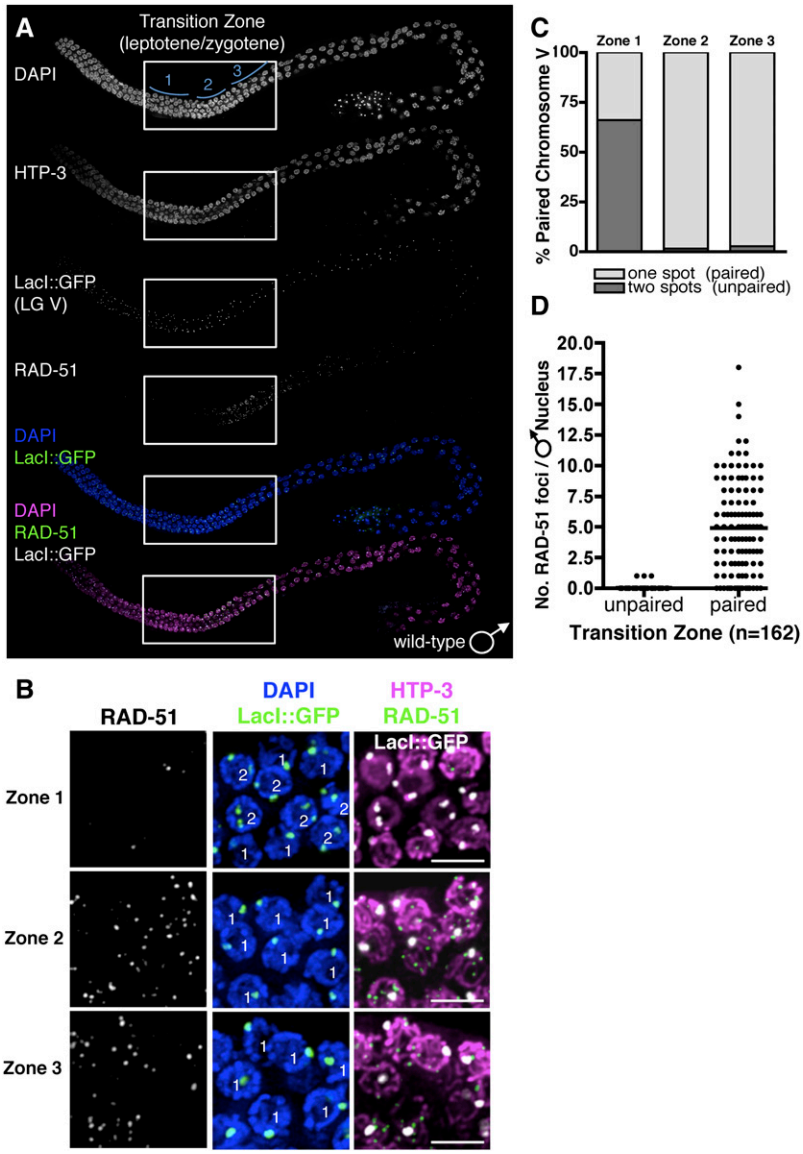

Figure 1 Homolog pairing and RAD-51 assembly are linked in the male germ line. (A) Wild-type male germ line carrying a LacO insertion on chromosome V (LacO-V) stained for HTP-3, RAD-51, and LacI-His$_6$-GFP and counterstained with DAPI. Rectangle indicates transition zone (TZ) stage nuclei identified by DAPI morphology. Zones 1–3 correspond to early, mid, and late TZ nuclei. Bar, 15 μm. Chromosome V pairing and RAD-51 kinetics in these nuclei were assessed in B. Left, RAD-51 foci are first detected in zone 1 and are detected on all nuclei by zone 2. Middle, DAPI (blue) and LacI-His$_6$-GFP (green) staining distinguish between paired (single focus) *vs.* unpaired (two distinct foci) chromosome V homologs. White numbers indicate number of LacI-His$_6$-GFP foci observed per nucleus. Right, axial element HTP-3 (magenta) accumulates on chromatin at the end of zone 1 coincident with chromosome pairing (LacI-His$_6$-GFP, white), and onset of RAD-51 assembly (green). Right, RAD-51 foci are first detected in zone 1 and are detected on all nuclei by zone 2. Bars, 5 μm. (C) Kinetics of homolog pairing were assessed by scoring LacI-His$_6$-GFP foci per nucleus in each zone (n = 163). (D) Quantification of RAD-51 foci in unpaired (n = 43; av = 0.07) *vs.* paired (n = 120; av = 4.93) TZ nuclei. Data were analyzed using a two-tailed Mann–Whitney test; $^{**}P < 0.0001$.

accumulate SPO-11-dependent RAD-51 foci in the TZ (Jaramillo-Lambert and Engebrecht 2010). In male germ lines, chromosome Vs were paired by early-to-mid TZ, coincident with the timing of RAD-51 assembly (Figure 1, B and C). Analysis of RAD-51 foci throughout the TZ revealed that only 7% of nuclei contained RAD-51 prior to chromosome V pairing (1 focus/nucleus), while in TZ nuclei with paired chromosome Vs, 86% contained one or more RAD-51 foci [average (av) = 4.93 foci/nucleus], indicating a strong bias toward RAD-51 assembly on paired homologs (Figure 1D).

In hermaphrodites, SC assembly takes place primarily in late TZ/EP nuclei (Colaiacovo *et al.* 2003). To assess the kinetics of SC assembly relative to homolog pairing in the male germ line, we next monitored the loading of the central element component SYP-1 (MacQueen *et al.* 2002) in LacO-V worms. In male germ cells, SYP-1 stretches first appeared in early TZ nuclei (Figure 2, A and B). Paired chromosome V homologs were detected almost exclusively in nuclei containing SYP-1 on all chromosomes, indicating that completion of SC assembly occurs coordinately on all chromosomes in males. Indeed, all homolog pairs contained a fully assembled SC by mid TZ (Figure 2, A, C, and D).

As homolog pairing and SC assembly is coincident with RAD-51 foci formation in males, we examined the status of the X chromosome in TZ nuclei. Surprisingly, we did not observe a chromosome lacking SYP-1 in several mid-to-late TZ stage nuclei (Figure 2, C and D, arrowhead), suggesting that SYP-1 was loaded on the X chromosome. To investigate this, we used SIM to assess loading of both SYP-1 and the axial component HTP-3, which accumulates on chromosomes in early TZ nuclei (Figure 1, A and B). In every male germ line examined (n = 18), we detected one to three mid-to-late TZ nuclei where we could unambiguously identify the X (by absence of H3K4me2) that contained a SYP-1 track (Figure 2, E–H). By EP, however, a single DAPI-stained body, presumably the X, was lacking SYP-1 (Figure 2A),

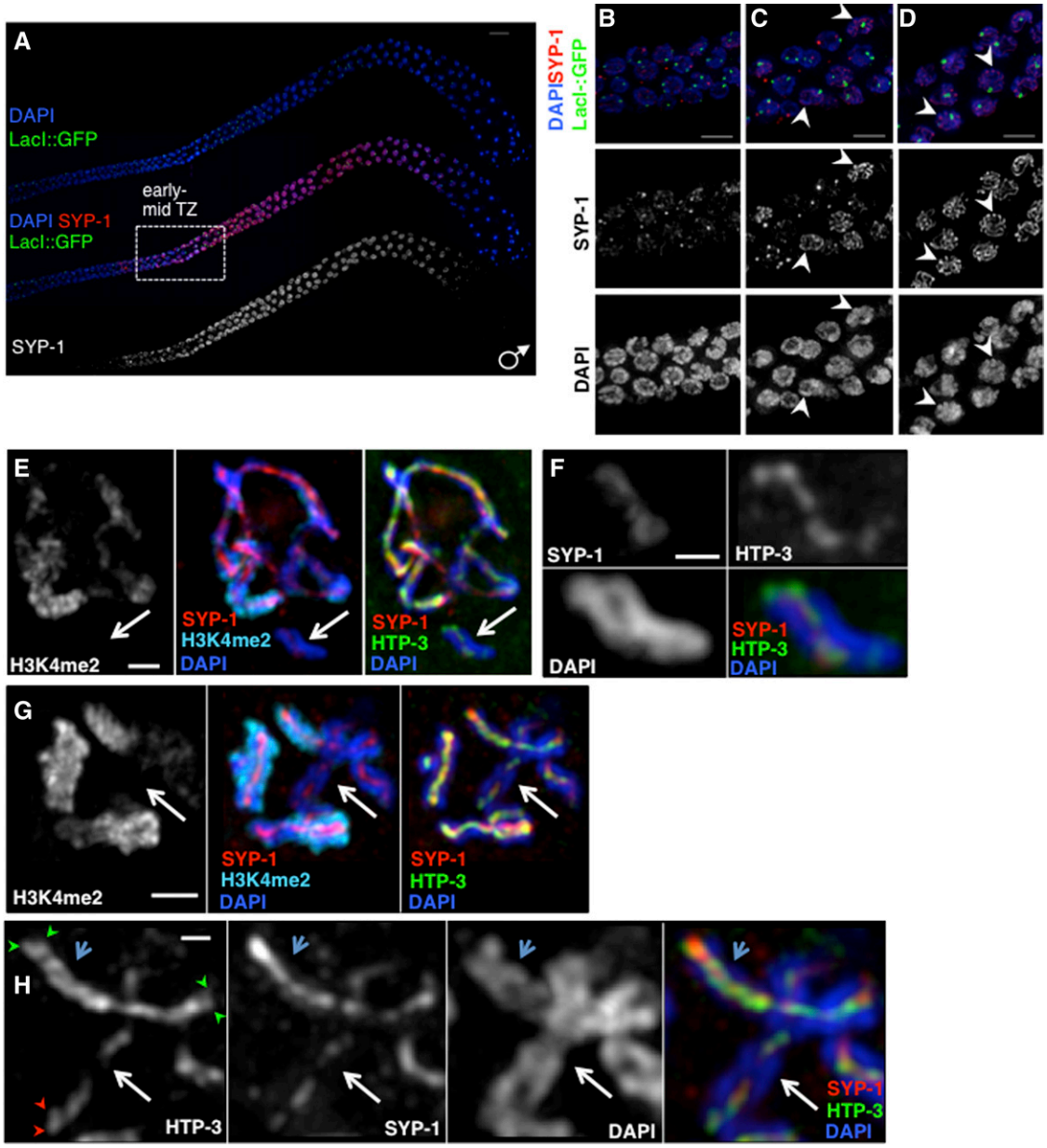

Figure 2 SYP-1 transiently loads onto the X chromosome of males coincident with RAD-51 assembly. (A) Wild-type male germ lines carrying a LacO insertion on chromosome V (LacO-V) were stained for SYP-1 (red, bottom) and LacI-His$_6$-GFP (green) and counterstained with DAPI (blue). Rectangle indicates region of early-mid TZ stage nuclei assessed in B–D. Bar, 15 μm. (B) Partial SYP-1 tracks are detected on chromatin in early TZ nuclei prior to chromosome pairing. (C and D) Chromosome V pairing is coincident with presence of SYP-1 on all chromosomes including presumably the X (white arrowheads); bars, 5 μm. (E and G) SIM images of male late TZ nuclei stained for SYP-1 (red), DAPI (blue), and H3K4me2 (cyan) or HTP-3 (green). White arrow indicates X chromosome, identified by lack of H3K4me2 staining. Bar, 5 μm. (F and H) Blow up of X chromosomes from E and G. In H, white arrow indicates the X chromosome and red arrowheads indicate two tracks of HTP-3; blue arrow indicates an autosome and light green arrowheads show two HTP-3 tracks. Bar, 1 μm. Images are partial projections with *Z* stacks acquired at 0.133-μm intervals.

suggesting that SYP-1 loads on the X only within a brief window coincident with onset of meiotic DSB formation.

As the X lacks a homolog, SYP-1 could be loaded onto regions of the X that have folded back on itself, assembled on a single axis, or loaded between the sister chromatids. The six *C. elegans* chromosomes are very similar in overall nucleotide length (*C. elegans* Sequencing Consortium 1998), although the X chromosome of males becomes highly condensed as meiosis proceeds (Bean *et al.* 2004; Checchi and Engebrecht 2011). We observed two classes of nuclei (n = 30) where SYP-1 tracks were present on the X: nuclei where the X appeared shorter and more compact than the autosomes (36.66%; Figure 2, E and F), consistent with fold-back synapsis, and nuclei where the X and autosomes were

comparable in length (63.33%; Figure 2, G and H), suggesting that SYP-1 is assembled on a single axis and/or loaded between the sisters. Further, in some nuclei with an extended X, two tracks of DAPI and HTP-3 could be distinguished (HTP-3; red arrowheads) similar to what was observed on autosomes (HTP-3; green arrowheads) (Figure 2H), suggesting that in these nuclei, SYP-1 is loaded between the sister chromatids.

Meiotic cohesin is altered on the X chromosome of males

A prediction based upon SYP-1 loading between the X sister chromatids is that sister chromatid cohesion (SCC) will also be altered. To investigate this, we first monitored the localization of the meiotic kleisins REC-8 and COH-3, which are essential for SCC during meiosis (Severson *et al.* 2009; Tzur *et al.* 2012). In hermaphrodites, REC-8 is nucleoplasmic in mitotic germ cells and localizes to chromatin in early meiotic prophase (Pasierbek *et al.* 2001; Severson *et al.* 2009). Similarly, we found that in males, REC-8 was visible in all mitotic germ cell nuclei and became concentrated on chromosomes upon entry to the TZ (Figure 3, A and B). COH-3 was not observed in mitotic germ cells but was recruited to chromatin in a similar pattern to REC-8 upon meiotic entry (Figure 3, C and D).

Whereas REC-8 and COH-3 were detected on autosomes beginning in early meiotic prophase, both REC-8 and COH-3 had an altered staining pattern on the X chromosome. REC-8 was detected on the X in TZ nuclei, yet COH-3 was only observed on autosomes at this stage (Figure 3, B and D). Interestingly, by early pachytene, the X was either devoid or contained significantly reduced levels of both REC-8 and COH-3 as compared to autosomes (Figure 3, B and D). By MP to late pachytene (LP), however, stretches of REC-8 and COH-3 became apparent on the X chromosome. As REC-8 and COH-3 staining was also present in spermatocyte nuclei where the X is very highly condensed, it is unlikely that the compacted nature of the X precludes antibody access at earlier stages. Furthermore, the same staining pattern was observed in *met-2* males (data not shown), which fail to load the repressive histone mark H3K9me2 on the X chromosome of males (Bessler *et al.* 2010; Checchi and Engebrecht 2011). Additionally, in males lacking ZIM-2, a protein required for chromosome V homolog pairing (Phillips and Dernburg 2006), robust staining was observed on the asynapsed chromosome Vs throughout pachytene, indicating that decreased REC-8/COH-3 staining on the X is not a consequence of having unpaired *vs.* paired homologs (Figure 3E). These results indicate that loading and accumulation of meiotic cohesin is altered on the X chromosome of males.

REC-8 and COH-3/4 are not required for RAD-51 removal on the X chromosome

The reduction/lack of REC-8 and COH-3 on the X chromosome of males in early prophase suggests that meiotic cohesin is not a requirement for DSB repair on the X. To test this, we monitored RAD-51 kinetics in mutants lacking REC-8 and COH-3/4. In wild-type male germ lines, RAD-51 foci are largely disassembled by mid pachytene (Figure S1), reflecting repair. In contrast, *rec-8*; *coh-3/4* male germ lines had abundant RAD-51 foci that persisted throughout meiotic prophase (Figure 4, A and B), suggesting that as in hermaphrodites (Tzur *et al.* 2012), DSB repair is impaired in males lacking meiotic kleisins. To determine whether RAD-51 disassembly is compromised on the X chromosome in *rec-8*; *coh-3/4* male germ lines, we compared the number of RAD-51 foci on the X chromosome in wild-type *vs.* *rec-8*; *coh-3/4* males (Figure 4B). We found no significant difference ($P = 0.081$) in the number of X chromosome-specific RAD-51 foci in late pachytene nuclei, suggesting that DSBs on the X can be repaired in the absence of meiotic kleisins.

We next examined the association of sister chromatids by FISH in males harboring a single copy lacO array on the X chromosome. As expected, both wild-type and *rec-8*; *coh-3/4* males contained predominantly a single FISH focus on the X in proliferative zone nuclei, indicative of cohesion between sisters presumably due to the presence of mitotic kleisins. In TZ, 5.0% of wild-type and 10.0% of *rec-8*; *coh-3/4* nuclei had two distinct foci ($P = 0.76$), suggesting that sister chromatid association is largely independent of meiotic kleisins at this stage of meiotic prophase. However, as pachytene progressed, *rec-8*; *coh-3/4* germ lines displayed increasing percentages of nuclei with two distinct foci compared to wild type [EP: 14 *vs.* 3.2% ($P = 0.0022$); MP: 18.1 *vs.* 5.6% ($P = 0.0072$); LP: 31.4 *vs.* 8.4% ($P < 0.0001$)] (Figure 4C). These results suggest that meiotic kleisins contribute to sister interactions during pachytene but are not required for meiotic DSB repair on the X chromosome of males.

SMC-5/6 facilitates DSB repair on autosomes but is dispensable for DSB repair on the X chromosome of males

Structural maintenance of chromosome proteins SMC-5 and SMC-6 (SMC-5/6) have been proposed to mediate sister chromatid recombination in the *C. elegans* hermaphrodite germ line (Bickel *et al.* 2010). *smc-5/6* hermaphrodites give rise to viable offspring, presumably because interhomolog (IH) repair is intact; however, a subset of RAD-51 foci persist through late pachytene (Bickel *et al.* 2010). To determine whether SMC-5/6 plays a role in recombinational repair on the X chromosome of males, we monitored RAD-51 kinetics in *smc-5/6* male germ lines and saw elevated numbers of RAD-51 foci throughout pachytene (Figure 5C and Figure S2A). Interestingly, RAD-51 did not accumulate to the same extent in *smc-5/6* males compared to hermaphrodites, suggesting that there are sex-specific constraints underlying meiotic DSB repair (Bickel *et al.* 2010) (Figure 5C and Figure S2A). Despite these differences, however, SMC-5/6 is important for male gamete quality, as there is

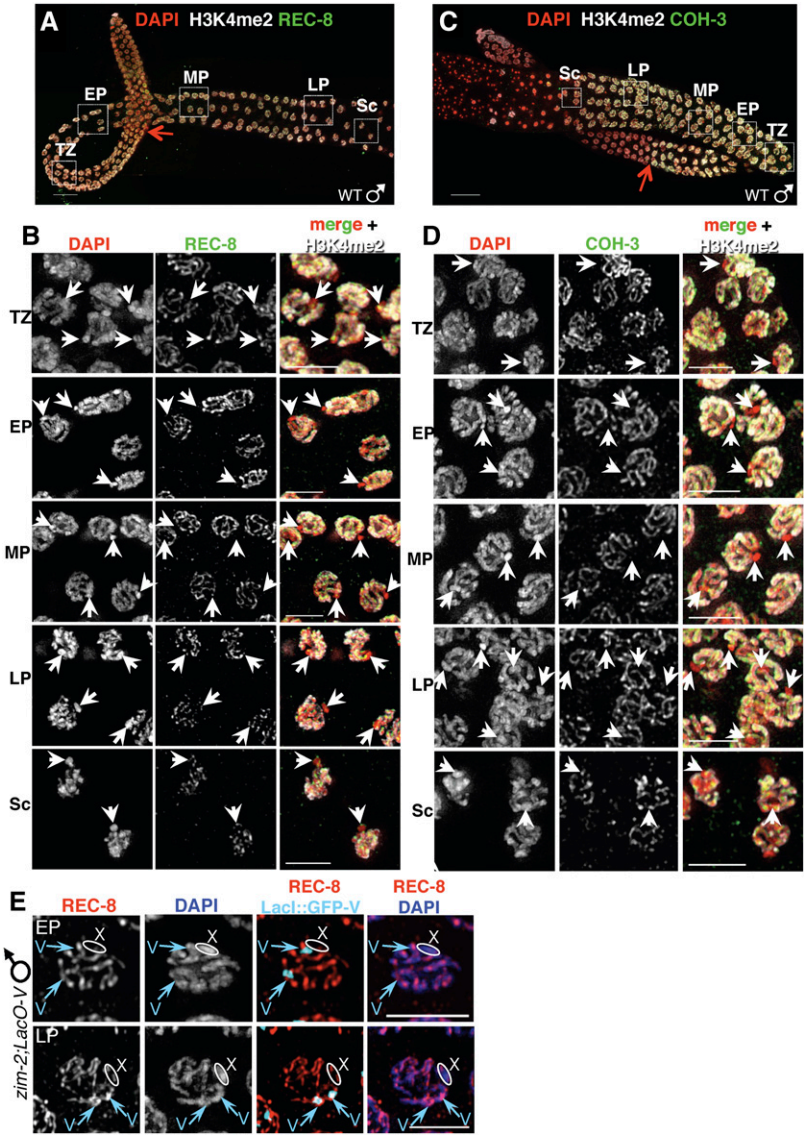

Figure 3 Kinetics of REC-8 and COH-3 assembly differ between the autosomes and the X in male germ lines. Localization of meiotic kleisins REC-8 (A and B) and COH-3 (C and D) were examined in wild-type male gonads. The X chromosome of males (white arrowheads) was identified by morphology and absence of H3K4me2 (white in merge). (A) REC-8 (green) is detected in the nucleoplasm throughout the proliferative zone (PZ) and accumulates on chromatin at the onset of the TZ (red arrow) (B) where it is detected on all chromosomes including the X (white arrowheads); H3K4me2 (white in merge). In early-mid pachytene (EP-MP) REC-8 staining is abundant on autosomes and present at very low levels on the X. By late pachytene-spermatocytes (LP/Sc) (B), REC-8 is visible on all chromosomes. (C and D) COH-3 is absent from the PZ and is first detected on chromatin at the onset of TZ, but is not detected on the X until LP/Sc (H3K4me2; white in merge). (E) In *zim-2* males REC-8 (red) readily accumulates on unpaired chromosome V homologs detected by LacI-His_6-GFP (cyan arrows) throughout pachytene, whereas the REC-8 staining on the X chromosome (white circles) is not abundant until LP. (A and C) Bars, 15 μm. (B, D, and E) Bars, 5 μm.

a 10% decrease in offspring survival among the progeny of females fertilized by *smc-5* male sperm (Figure S3A).

As IH repair cannot be engaged on the partnerless X chromosome of males, we asked whether RAD-51 foci persisted on the X chromosome in the absence of SMC-5/6. Surprisingly, we found no significant difference in the number of RAD-51 foci on the X chromosome of *smc-5/6* mutant males as compared to wild type ($P = 0.4269$; Figure 5D and Figure S2B), suggesting that SMC-5/6 is not required for DSB repair on the X chromosome.

Similar to the X chromosome of males, asynapsed autosomes also lack the ability to repair DSBs via IH repair (Bickel *et al.* 2010). We therefore tested whether absence of SMC-5/6 impaired RAD-51 removal in *zim-2* males. Indeed, *smc-6*; *zim-2* males contained elevated RAD-51 foci that persisted on the unpaired chromosome Vs throughout late pachytene/spermatocyte (LP/Sc) stage, longer than in either single mutant on its own (Figure 5B and Figure S2, C–K). These results indicate that while SMC-5/6 is required for DSB repair on autosomes when a homolog is unavailable in the male germ line, the constitutively unpaired X chromosome can repair meiotic DSBs in the absence of SMC-5/6.

Absence of SMC-5/6 increases chromosome fragmentation of asynapsed X chromosomes of hermaphrodites but not the X chromosome of males

Another consequence of unrepaired DSBs is chromosome fragmentation, which manifests in loss of genetic material, aneuploid gametes, and inviable offspring (Aguilera and Garcia-Muse 2013). In *smc-5* hermaphrodites, chromosome fragments are apparent in oocyte nuclei that form crossovers, indicating a propensity toward chromosome loss even in the presence of successful IH repair (Bickel *et al.* 2010).

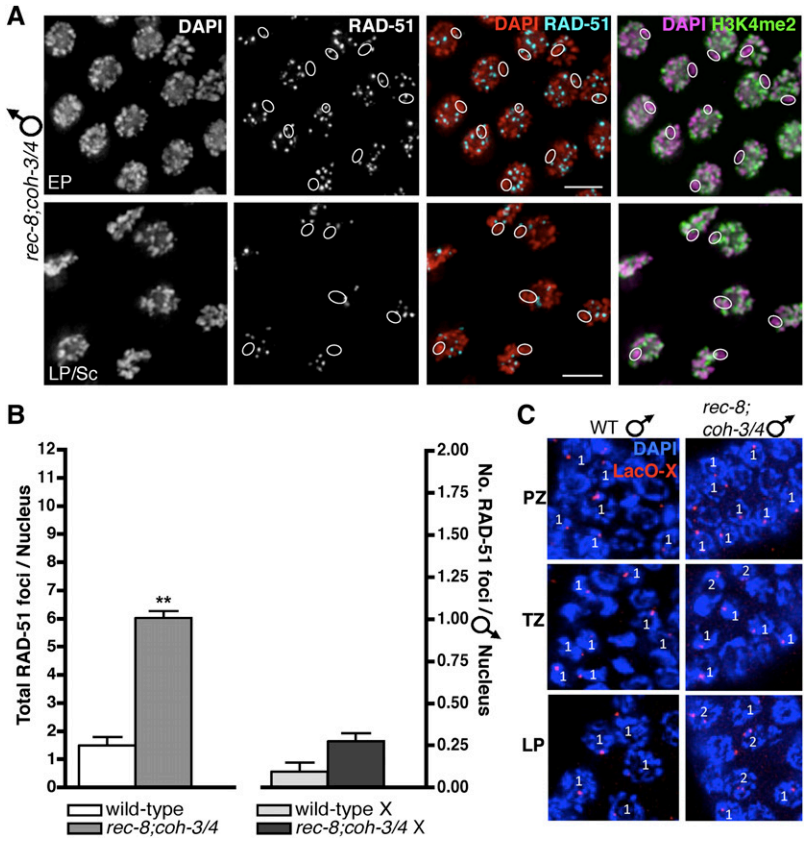

Figure 4 Meiotic kleisins are not essential for RAD-51 removal on the X chromosome of males. (A) Early-stage (left column) and late-stage (right column) pachytene *rec-8(ok978)*; *coh-3(gk112)coh-4(tm1857)* male nuclei co-stained with RAD-51 (cyan in merge) and H3K4me2 (green; to distinguish the X) and counterstained with DAPI. White circle denotes X chromosome. Bars, 5 μm. (B) Total RAD-51 foci (left) and X chromosome-specific RAD-51 foci (right) were scored in wild type (n = 43) *vs.* *rec-8*; *coh-3/4* (n = 113) LP/Sc stage male nuclei. Data were analyzed using a two-tailed Mann–Whitney test; $^{**}P < 0.0001$. Comparison of total RAD-51 foci per nucleus: wild type (av = 1.49 ± 0.29) *vs.* *rec-8*; *coh-3/4* (av = 6.03 ± 0.24), $P < 0.0001$. Comparison of RAD-51 foci per X chromosome: wild type (av = 0.09 ± 0.06) *vs.* *rec-8*; *coh-3/4* (av = 0.27 ± 0.05), $P = 0.081$. (C) X chromosome-specific RAD-51 foci were scored in wild-type (n = 43) *vs.* *rec-8*; *coh-3/4* (n = 113) LP/Sc stage male nuclei. Data were analyzed using a two-tailed Mann–Whitney test; $P = 0.081$. Bars, 5 μm. (C) FISH detection of a X chromosome-specific LacO insertion (red) in wild-type and *rec-8*; *coh-3/4* male germ line nuclei. White numbers indicate number of FISH foci observed per nucleus. Data were analyzed using the Fisher's exact test: PZ nuclei with two spots: 6.1% wild type (n = 98), 11.6% *rec-8*; *coh-3/4* (n = 129), P = 0.1734; TZ nuclei with two spots: 5.0% wild type (n = 262), 10.0% *rec-8*; *coh-3/4* (n = 120), P = 0.76; EP nuclei with two spots: 3.2% wild type (n = 289), 14% *rec-8*; *coh-3/4* (n = 143), P = 0.0022; MP nuclei with two spots: 5.6% wild type (n = 289), 18.1% *rec-8*; *coh-3/4* (n = 127), P = 0.0072; and LP nuclei with two spots: 8.4% wild type (n = 289), 31.4% *rec-8*; *coh-3/4* (n = 101), $P < 0.0001$. Bar, 10 μm.

We therefore asked whether absence of SMC-5 resulted in X chromosome loss in males, which would be predicted to increase the percentage of "nullo" sex chromosome (0) gametes. As sex is determined by the ratio of X chromosomes to autosomes in *C. elegans* (Zanetti and Puoti 2013), an increase in nullo sex chromosome gametes would in turn increase the percentage of male offspring when crossed with female (X containing) gametes. Despite a significant reduction in progeny viability, however, we observed no increase in the percentage of male offspring when *fog-2* females, which do not produce self sperm (Schedl and Kimble 1988), were mated to *smc-5* males, consistent with SMC-5/6 being dispensable for break repair on the X chromosome of males (Figure S3B).

To further investigate whether SMC-5/6 plays a role in DSB repair on the X chromosome, we depleted *smc-6* by RNAi and assessed chromosome fragmentation. We first tested whether X chromosome asynapsis caused by the *him-8* mutation (Phillips and Dernburg 2006) enhanced the *smc-6(RNAi)* phenotype. In *smc-6(RNAi)*; *him-8* XX germ lines 56% of nuclei contained fragmented chromosomes (n = 36) *vs.* 29% in *smc-6(RNAi)* XX alone (n = 31) and 4% in *him-8* XX single mutants (n = 47) ($P < 0.0001$; Figure 6E). These data corroborate previous observations that SMC-5/6 activity is specific to intersister recombination, and that depletion of this complex is highly deleterious in situations where a homolog is unavailable as a repair template (Bickel *et al.* 2010).

In the hermaphrodite germ line, chromosome fragmentation is readily detected in diakinesis (DI) nuclei as chromosomes at this stage are condensed, and in wild-type hermaphrodites all six bivalents are physically separated from each other throughout the oocyte (Schvarzstein *et al.* 2010). However, nuclei in the equivalent stage of male meiosis (spermatocytes/sperm) are very highly compacted, which precludes identification of fragmented chromosomes. To circumvent this, we assessed fragmentation in heterogametic *fem-3* X0 females, which have a feminized germ line but possess a single X chromosome with properties similar to the X chromosome of males (Hodgkin 1986; Jaramillo-Lambert and Engebrecht 2010; Checchi and Engebrecht 2011). We depleted *smc-6* by RNAi in *fem-3* X0 females, and in both control (empty vector) and *smc-6(RNAi)*; *fem-3* X0 germ lines, we were able to identify the X by its smaller size and compact morphology (Figure 6, A–D). Whereas six DAPI bodies (five bivalents and the univalent X) were observed in all control *fem-3* X0 DI stage nuclei, we observed at least seven DAPI bodies in 16% of *smc-6(RNAi)*; *fem-3* X0 germ lines scored (Fisher's exact test P = 0.0002). In contrast, fragmented nuclei

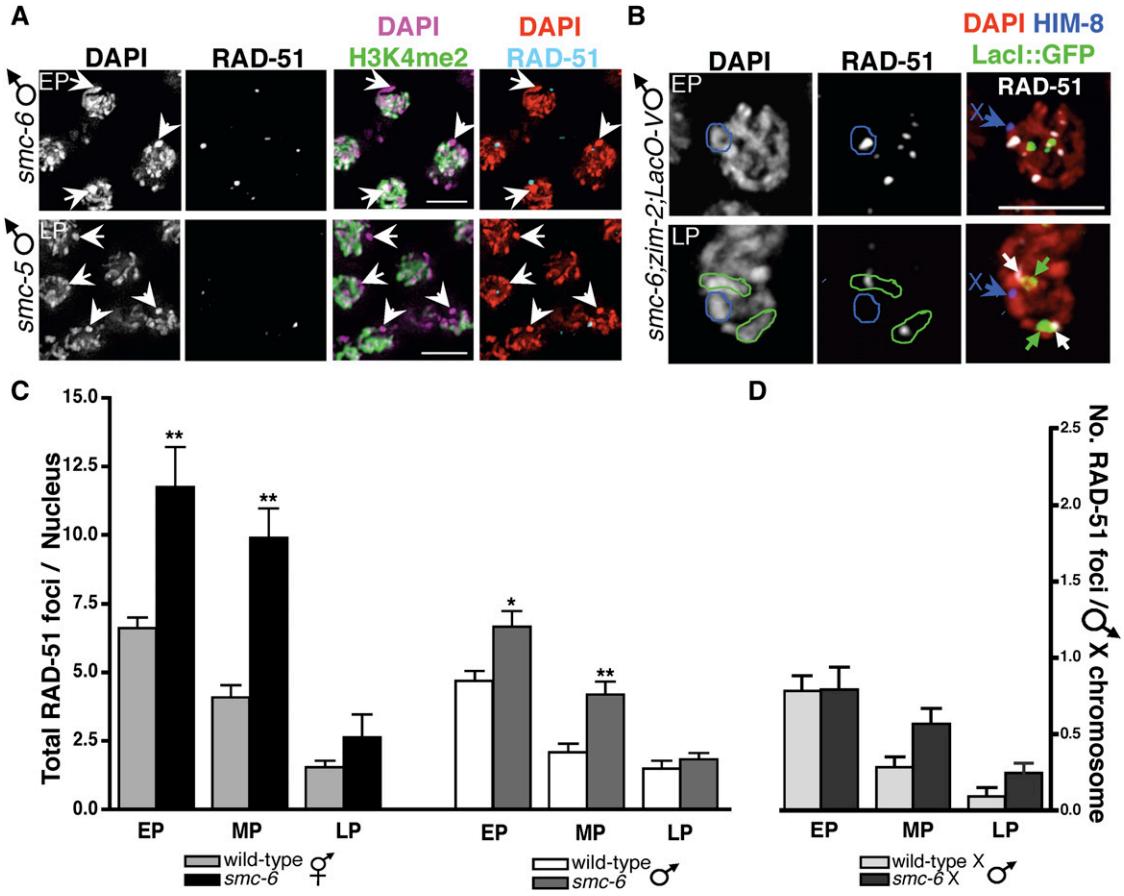

Figure 5 Structural maintenance of chromosome complex SMC-5/6 is dispensable for RAD-51 removal on the X chromosome of males. (A) RAD-51 foci (cyan in merge) were assessed in male *smc-6(ok3294)* (top) and *smc-5(ok2421)* (bottom) late pachytene-spermatocyte (LP/Sc) nuclei. Gonads were co-stained with H3K4me2 (green) and DAPI. White arrowheads denote the X chromosome. Bars, 5 μm. (B) In an EP *smc-6(ok3294)*; *zim-2(tm574)*; *LacO-V* nucleus RAD-51 foci (white in merge) were detected on all chromosomes including the X, identified by HIM-8 staining (blue focus, arrow/circles) and the unpaired chromosome Vs (LacI-His_6-GFP, green). In a LP nucleus RAD-51 foci (white arrows) persist on the asynpased Vs (green arrows/circles) but not the X (blue arrow/circles). (C and D) Total (C) and X-specific (D) RAD-51 in wild-type and *smc-6* germ lines throughout pachytene. Data were analyzed using a two-tailed Mann–Whitney test. $*P < 0.01$; $**P < 0.001$. Error bars = SEM (see also Figure S2). Comparison of total DSBs/nucleus during pachytene: wild-type XX ($n = 336$, av = 4.92 ± 0.26) *vs. smc-6* XX ($n = 61$, av = 8.75 ± 0.81), $P = 0.0002$; wild-type X0 ($n = 202$, av = 2.98 ± 0.22) *vs. smc-6* X0 ($n = 198$, av = 3.89 ± 0.28), $P = 0.0217$. Comparison of DSBs/X chromosome: wild-type X0 ($n = 183$, av = 0.40 ± 0.05) *vs. smc-6* X0 ($n = 198$, av = 0.50 ± 0.05), $P = 0.4269$.

were observed in 47% of *smc-6(RNAi)*; *fem-3* XX germ lines, which was significantly higher than either *fem-3* XX controls or *smc-6(RNAi)*; *fem-3* X0 germ lines ($P < 0.0001$; Figure 6E). These data suggest that the excess DAPI bodies observed in *smc-6(RNAi)*; *fem-3* X0 nuclei were most likely fragmented autosomes and not a consequence of unrepaired DSBs on the X. Taken together, the lack of impairment of DSB repair on the X chromosome of *C. elegans* males in the absence of both REC-8/COH-3/4 and SMC-5/6 in combination with the cytology suggests that X sister chromatids are configured to mimic homologs early during meiotic prophase.

COM-1 is required for DSB processing on all chromosomes in the male germ line

In wild-type males, a COSA-1 focus, which marks the site COs (Yokoo *et al.* 2012) is detected on all chromosomes except the X, indicating this is the only chromosome that does not form a CO (Figure S4). To determine whether absence of a crossover on the X reflects altered DSB repair pathway selection, we examined RAD-51 localization in *com-1* males. *C. elegans* hermaphrodite germ cells are characterized by a robust HR bias wherein the CtIP homolog COM-1 blocks error-prone NHEJ and promotes IH repair to ensure CO formation; in the absence of COM-1, very few RAD-51 foci are observed as DSBs are shunted through NHEJ (Lemmens *et al.* 2013). As in hermaphrodites, *com-1* male germ lines contained substantially fewer RAD-51 foci on all chromosomes, including the X, as compared to wild-type nuclei (Figure 7), which presumably reflects repair of induced DSBs through NHEJ (Lemmens *et al.* 2013). These data indicate that despite the absence of a homolog, a robust COM-1-mediated HR bias remains intact on the hemizygous X chromosome.

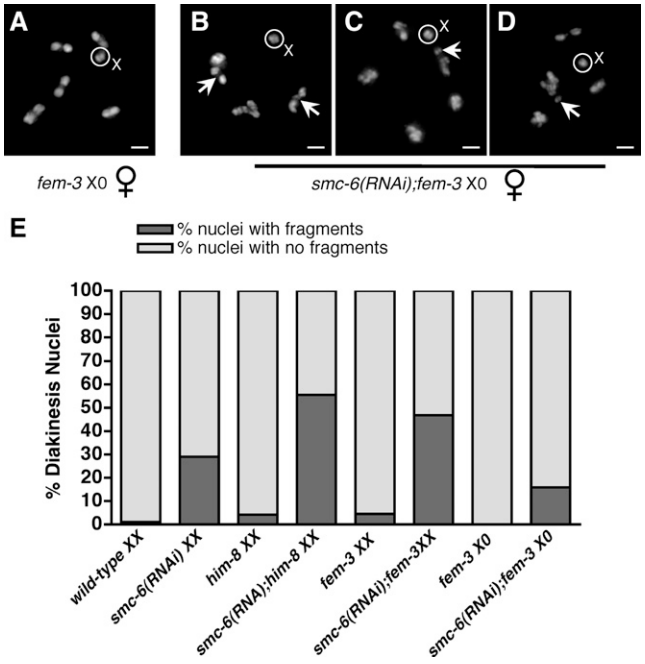

Figure 6 Loss of SMC-6 induces fragmentation on autosomes and asynapsed X chromosomes but not the X chromosome of males. (A) DAPI stained chromosomes in a *fem-3(e1996)* X0 diakinesis (DI) −1 oocyte reveals five bivalents and a single X chromosome identified morphologically (white circles). Bars, 5 μm. (B–D) *smc-6* depletion induces fragmentation (white arrows) in *fem-3* X0 −1 DI nuclei. (E) Fragmented (dark gray) *vs.* unfragmented (light gray) nuclei in wild type *vs. him-8* and *fem-3* single and combinatorial mutants. Data were analyzed using a Fisher's exact test: wild-type XX, $n = 91$ *vs. smc-6(RNAi)* XX, $n = 31$: $P < 0.0001$; *him-8* XX, $n = 47$ *vs. smc-6(RNAi)*; *him-8* XX, $n = 36$: $P < 0.0001$; *fem-3* (L4440) XX, $n = 152$ *vs. smc*-6(RNAi); *fem-3* XX, $n = 226$: $P < 0.0001$; *fem-3* X0 (L4440), $n = 70$ *vs. smc-6(RNAi)*; *fem-3* X0 ($n = 101$): $P = 0.0002$; *smc-6(RNAi)*; *fem-3* XX *vs. smc-6(RNAi)*; *fem-3* X0, $P < 0.0001$.

The X chromosome of males is the only chromosome not subject to ATM-1-dependent feedback mechanisms at the level of DSB formation

Recent studies have uncovered feedback mechanisms proposed to monitor homolog pairing and DSB formation and to ensure timely CO formation (Barchi *et al.* 2008; Carballo *et al.* 2013; Kauppi *et al.* 2013; Rosu *et al.* 2013; Stamper *et al.* 2013). We speculated that in the heterogametic sex, such feedback mechanisms are altered to handle the challenges of a constitutively unpaired chromosome. In yeast and mice, the ataxia telangiectasia mutated (ATM) kinase plays a role in the establishment and maintenance of feedback mechanisms that ensure DSB homeostasis; in the absence of ATM more DSBs are formed (Carballo *et al.* 2013; Kauppi *et al.* 2013). To address the role of feedback mechanisms in the regulation of the hemizygous X, we first monitored RAD-51 kinetics in *C. elegans* mutants deficient for ATM-1. We found that both hermaphrodite and male *atm-1* mutants contained more RAD-51 foci throughout meiotic prophase than wild type (Figure 7, A and C–E), suggesting that ATM-1 is important for inhibiting DSB formation once a CO precursor has formed on every chromosome.

Elevated RAD-51 could be a consequence of a greater number of DSBs formed, an extended period of break formation, and/or slower turnover. *rad-54* mutants have been used to distinguish between increased number of DSBs *vs.* a defect in repair as RAD-54 is essential for RAD-51-mediated strand exchange during HR and is required for RAD-51 disassembly (Solinger *et al.* 2002; Mets and Meyer 2009). However, recent work indicates that absence of RAD-54 both impedes RAD-51 turnover and also extends the time for which DSBs are formed (Rosu *et al.* 2013; Stamper *et al.* 2013). To elucidate the underlying cause of elevated RAD-51 foci in *atm-1* mutants, we analyzed RAD-51 foci in *rad-54*; *atm-1(RNAi)* male germ lines. We found an even greater number of foci in *rad-54*; *atm-1(RNAi)* than either *atm-1* or *rad-54* mutants alone (Figure 7 and Figure S5), suggesting that ATM-1 regulates the number of DSBs formed independent of the extension of time when breaks are formed in *rad-54* mutants.

In mice, ATM is also required for multiple aspects of sex chromosome regulation including the X-Y crossover (Barchi *et al.* 2008). To test whether the X chromosome of males is subject to ATM-dependent DSB regulation, we next assessed RAD-51 levels on the X in the absence of ATM-1. In *atm-1* male germ lines, the X was the only chromosome that did not contain increased RAD-51 foci (Figure 7D), suggesting that the complete absence of a pairing partner relieves the *C. elegans* X chromosome of males from these constraints. Together these results suggest that although early processing of breaks is similar between autosomes and the X, later steps are altered to accommodate the absence of a homolog.

HR is essential for RAD-51 disassembly on all chromosomes except the X chromosome of males

To examine subsequent steps in DSB processing, we monitored RAD-51 kinetics in the absence of RAD-54. In *rad-54* males, RAD-51 was detected on all chromosomes including the X in early meiotic prophase (mid TZ stage), indicating that the X chromosome is competent for DSB formation in the absence of RAD-54 (Figure 8, A and B). By pachytene, RAD-51 foci were abundant on the autosomes, but the X chromosome was largely devoid of foci in *rad-54* males (Figure 8B). We did observe nuclei where one to two RAD-51 foci were retained on the X, suggesting that RAD-54 does facilitate break repair on all chromosomes. However, RAD-51 was disassembled on at least a subset of X DSBs (Figure 8C), as a significantly smaller percentage of the total RAD-51 foci localized to the X during pachytene [2% in *rad-54 vs.* 14% (one-sixth) in wild-type males; Figure 8D]. Further, a single pair of autosomes contained upwards of five times as many RAD-51 foci as compared to the X (Figure 8E). These data suggest that unlike the autosomes, the X chromosome of males is at least partially competent for meiotic DSB repair in the absence of HR. To determine whether this phenotype

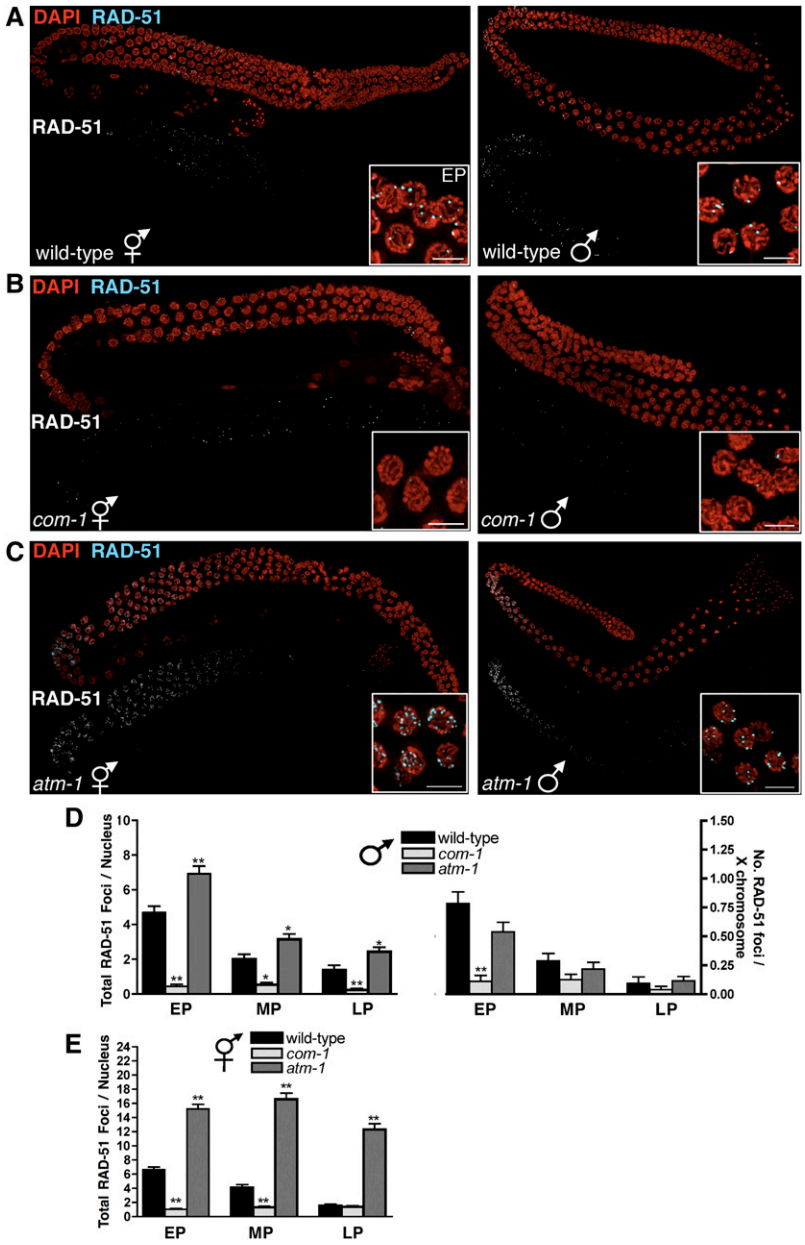

Figure 7 The X chromosome of males is subject to COM-1 but not ATM regulation. Whole-mount (A) wild-type, (B) *com-1(t1489)*, and (C) *atm-1(gk186)* germ lines stained with RAD-51 (cyan) and counterstained with DAPI (red). Insets are EP stage nuclei from these germ lines. Bars, 5 μm. (D) Quantification of total (left) and X chromosome-specific (right) RAD-51 foci in wild-type (n = 183), *com-1* (n = 168), and *atm-1* (n = 234) male germ line nuclei. Comparison of total RAD-51 foci per male nucleus: EP: wild-type (av = 4.6 ± 0.36), *com-1* (av = 0.43 ± 0.13), *atm-1* (av = 6.92 ± 0.44); MP: wild type (av = 2.0 ± 0.28), *com-1* (av = 0.53 ± 0.12), *atm-1* (av = 3.15 ± 0.31); LP: wild type (av = 1.38 ± 0.27), *com-1* (av = 0.24 ± 0.08), and *atm-1* (av = 2.44 ± 0.25). Comparison of total RAD-51 foci per male X chromosome: EP: wild type (av = 0.78 ± 0.10), *com-1* (av = 0.11 ± 0.05), *atm-1* (av = 0.54 ± 0.08); MP: wild-type (av = 0.29 ± 0.06), *com-1* (av = 0.13 ± 0.05), *atm-1* (av = 0.22 ± 0.06); LP: wild-type (av = 0.09 ± 0.06), *com-1* (av = 0.04 ± 0.03), and *atm-1* (av = 0.11 ± 0.04). (E) Quantification of total RAD-51 foci in wild-type (n = 336), *com-1* (n = 286), and *atm-1* (n = 185) hermaphrodite germ line nuclei. Data were analyzed using a two-tailed Mann–Whitney test. $*P < 0.01$ $**P \leq 0.0001$. Error bars = SEM.

also occurred in hermaphrodites carrying unpaired X chromosomes, we assessed RAD-51 kinetics in *rad-54*; *him-8* XX germ lines. We found that RAD-51 readily accumulated on all *rad-54*; *him-8* chromosomes including the unpaired Xs in the hermaphrodite germ line (Figure S6A). These data indicate that only DSBs on the X chromosome of males can be repaired when HR is blocked.

XPF-1 contributes to repair of meiotic DSBs on the X in the absence of HR

Our data reveal that DSB repair on the X chromosome of *C. elegans* males as monitored by RAD-51 disassembly can still occur in the absence of HR, indicating that additional pathways are available to repair DSBs on the X. To determine whether error-prone repair pathways contribute to DSB repair on the X chromosome of males, we monitored RAD-51 accumulation in mutants defective for NHEJ (*lig-4*; Clejan *et al.* 2006) or SSA (*xpf-1*; Saito *et al.* 2009) in the presence and absence of HR (*rad-54*). The number and kinetics of RAD-51 foci in *lig-4* or *xpf-1* single or double mutant germ lines were similar to wild type, both genome-wide and on the X (Figure S7). The total number of RAD-51 foci was also not significantly different in any of the double or triple mutant combinations compared to the elevated levels observed in *rad-54* male germ lines (Figure 9A). Further, inactivation of NHEJ in the absence of HR did not alter the number of RAD-51 foci observed on the X (*rad-54*; *lig-4*; Figure 9, B and C). In contrast, there was a significant increase in RAD-51 foci on the X chromosome in the *rad-54*; *xpf-1* double mutant (Figure 9, B and C). As an additive effect was not

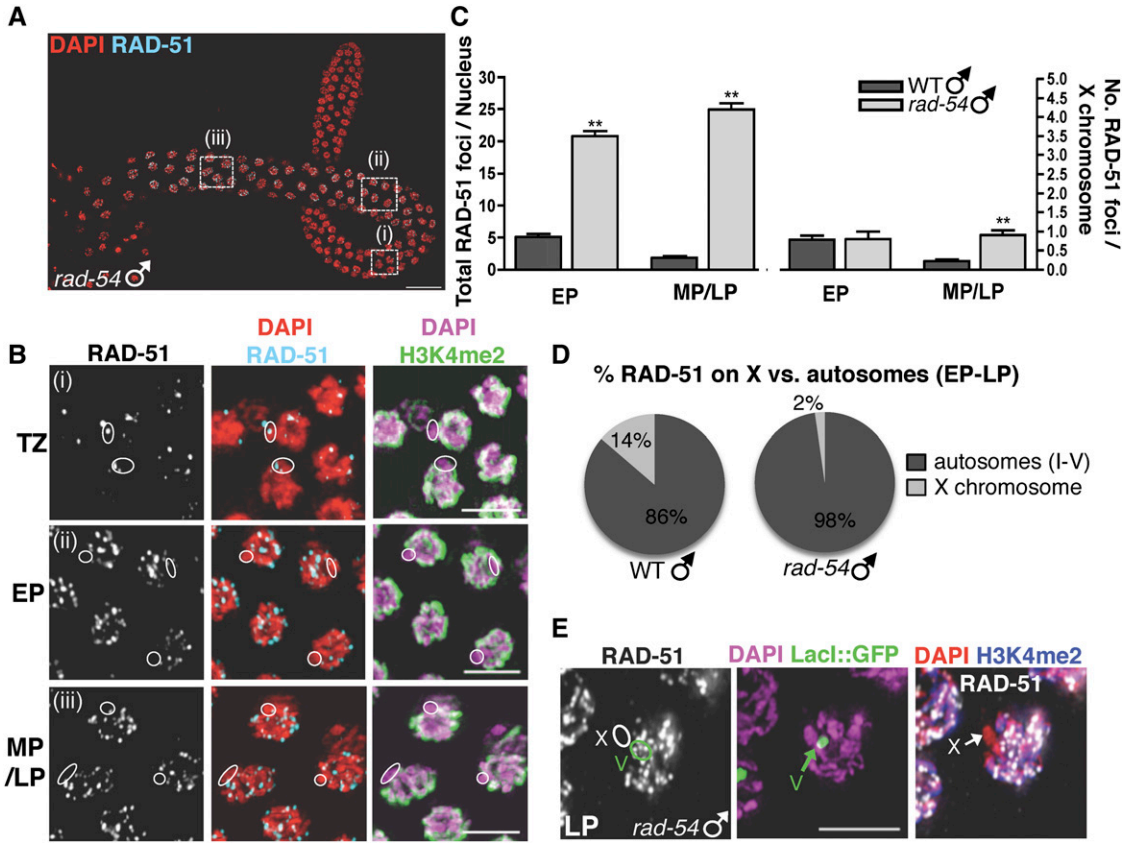

Figure 8 RAD-51 disassembly on the X in the absence of RAD-54. (A) Whole-mount *rad-54(ok615); him-8(me4)* male gonad stained with RAD-51 (cyan) and counterstained with DAPI (red). Bar, 15 μm. Dashed boxes correspond to TZ, EP, and MP/LP regions shown in B. White ovals indicate the X chromosome, which accumulates RAD-51 foci in the TZ (top row). By pachytene (middle-bottom panels), RAD-51 foci are predominant on autosomes while most are disassembled from the X. Bars, 5 μm. (C) Comparison of total RAD-51 (left) and RAD-51 on the X chromosome (right) from wild-type (n = 183) *vs. rad-54*; *him-8* male pachytene nuclei (n = 92). Data were analyzed using a two-tailed Mann–Whitney test. Error bars = SEM. $^{**}P < 0.0001$. Comparison of total DSBs/male nucleus: EP: wild-type (av = 5.15 ± 0.43) *vs. rad-54*; *him-8* (av = 20.77 ± 0.84); and MP/LP: wild type (av = 1.89 ± 0.22) *vs. rad-54*; *him-8* (av = 24.99 ± 0.96). Comparison of DSBs/male X chromosome: EP: wild type (av = 0.78 ± 0.10) *vs. rad-54*; *him-8* (av = 0.80 ± 0.20); and MP/LP: wild-type (av = 0.22 ± 0.05) *vs. rad-54*; *him-8* (av = 0.91 ± 0.11). (D) Pie graphs comparing percentage of RAD-51 foci on the male X *vs.* the autosomes in wild-type (left, 14% of DSBs on the X; 86% on autosomes) *vs. rad-54*; *him-8* males (right, 2% of DSBs on the X; 98% on autosomes). (E) *rad-54*; *him-8*; *LacO-V* male nucleus stained with LacI-His_6-GFP (green), H3K4me2 (blue), and RAD-51 (white) and counterstained with DAPI (red). Bars, 5 μm.

observed in either *rad-54*; *xpf-1*; *lig-4* or *rad-54*; *xpf-1*; *cku-80* triple mutants, these data indicate that following RAD-51 loading, SSA but not NHEJ contributes to X-specific break repair in the absence of HR. Taken together, these results suggest that an XPF-1-dependent SSA pathway can be engaged to repair breaks on the hemizygous X chromosome when HR is unavailable.

The tumor suppressor BRCA2 functions in HR by facilitating the loading of RAD-51 (Holloman 2011). In *C. elegans* *brc-2* mutants, HR is blocked and consequently the single-strand binding protein RPA-1 accumulates at breaks (Martin *et al.* 2005). Additionally, BRC-2 has been suggested to play a role in SSA (Martin *et al.* 2005). We therefore monitored the accumulation of RPA-1::GFP and RPA-1::YFP in the absence of BRC-2. Surprisingly, RPA-1::GFP and RPA-1::YFP foci accumulated in late pachytene nuclei in *brc-2* mutant males on all chromosomes except the X (Figure 10), suggesting that similar to RAD-54, BRC-2 is not absolutely essential for DSB repair on the X chromosome. Further, this is specific for the X chromosome of males as the asynapsed X chromosomes in *brc-2*; *him-8* hermaphrodites accumulated RPA-1::GFP (Figure S6B). To determine whether XPF-1 contributes to DSB repair on the X chromosome in the absence of BRC-2, we monitored RPA-1::GFP foci in *xpf-1*; *brc-2* double mutants and found that disassembly of RPA-1::GFP was significantly delayed on the X (Figure 10). Taken together, these results suggest that in the absence of either RAD-54 or BRC-2, XPF-1 mediates DSB repair on the hemizygous X chromosome.

Discussion

Here we uncover one strategy for how meiosis is altered to accommodate hemizygous sex chromosomes. In *C. elegans*

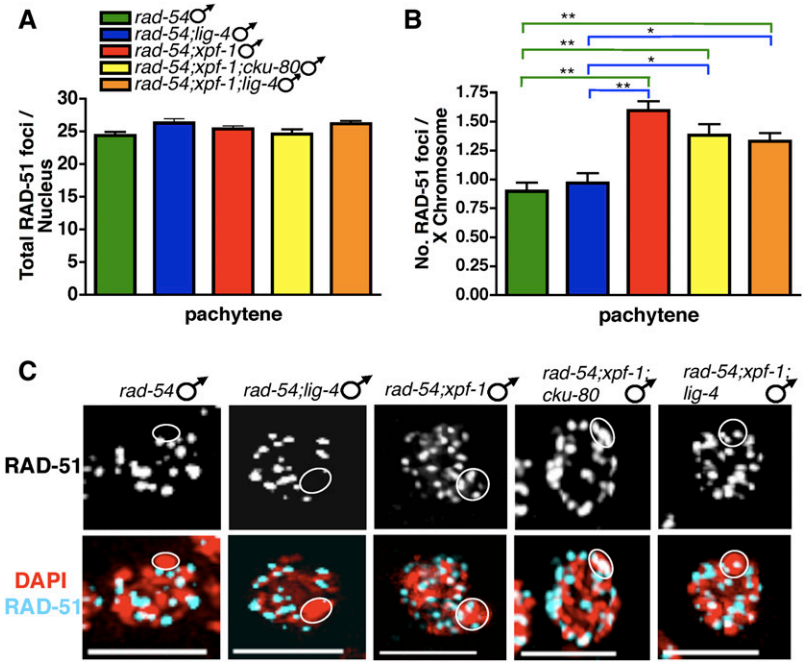

Figure 9 XPF-1 promotes RAD-51 disassembly on the X chromosome of males in the absence of HR. (A) Average number of RAD-51 foci per nucleus or (B) per X chromosome in pachytene male germ lines deficient for HR alone [*rad-54(ok615)*; *him-8(me4)*] or in combination with mutations in NHEJ [*lig-4(ok716)* and *cku-80(ok861)*], SSA [*xpf-1(ok3039)*], or both. Comparison of total RAD-51 foci per male nucleus: *rad-54*; *him-8*, n = 169 (av = 24.41 ± 0.52); *rad-54*; *lig-4*; *him-8*, n = 131 (av = 26.31 ± 0.66); *rad-54*; *xpf-1*; *him-8*, n = 226 (av = 25.40 ± 0.49); *rad-54*; *xpf-1*; *cku-80*; *him-8*, n = 120 (av = 24.62 ± 0.70); and *rad-54*; *xpf-1*; *lig-4*; *him-8*, n = 226 (av = 26.21 ± 0.42). Comparison of total RAD-51 foci per X chromosome: *rad-54*; *him-8*, n = 169 (av = 0.90 ± 0.07); *rad-54*; *lig-4*; *him-8*, n = 131 (av = 0.97 ± 0.09); *rad-54*; *xpf-1*; *him-8*, n = 226 (av = 1.60 ± 0.08); *rad-54*; *xpf-1*; *cku-80*; *him-8*, n = 120 (av = 1.38 ± 0.09); and *rad-54*; *xpf-1*; *lig-4*; *him-8*, n = 226 (av = 1.33 ± 0.07). Data were analyzed using a two-tailed Mann–Whitney test. $*P < 0.01$. $**P \leq 0.0001$. Error bars = SEM. (C) Representative examples of pachytene nuclei corresponding to mutants in A and B. Nuclei were stained with RAD-51 (cyan in merge) and counterstained with DAPI (red). The X chromosome is circled in white. Bars, 5 μm.

males, both the chromosome scaffold and the stringency of repair pathway choice have been modified to ensure that the completely hemizygous X chromosome is transmitted intact through meiosis.

Sister vs. homolog interactions and meiotic DSB formation

Analysis of the temporal relationship between chromosome pairing, synapsis, and DSB formation revealed that these events are tightly linked in the male germ line. DSBs, as monitored by the loading of the recombinase RAD-51, are invariably observed on paired and synapsed chromosomes (Figure 1 and Figure 2). Although these events can be uncoupled by mutational analyses in *C. elegans* (Dernburg *et al.* 1998) (Figure 8 and data not shown), the strict temporal relationship suggests that these events are normally interdependent. The interdependence of these events in *C. elegans* is also suggested by analyses of both the axial protein HTP-3, which links DSB formation with homolog pairing and synapsis (Goodyer *et al.* 2008) and CRA-1, whose inactivation uncovers a requirement for synapsis in DSB repair (Smolikov *et al.* 2008).

Our studies of the relationship between homolog pairing, synapsis, and RAD-51 assembly in the male germ line revealed a transient window whereby SYP-1 is loaded on the X chromosome concomitant with initiation of meiotic DSBs. Previous studies have indicated that loading of central element components is not dependent on homology *per se* and that SYP-1 can be loaded between nonhomologous chromosomes (Couteau and Zetka 2005; Martinez-Perez and Villeneuve 2005), on individual unpaired chromosomes (Smolikov *et al.* 2008; Zhang *et al.* 2012) or between regions of the same chromosome that have folded back on itself (Harper *et al.* 2011). While male germ line cytology is less favorable than in hermaphrodites (Jaramillo-Lambert *et al.* 2010; Checchi and Engebrecht 2011; Woglar *et al.* 2013) and SYP-1 is only detected on the X in TZ nuclei, where chromosomes are not well separated and therefore difficult to distinguish as individual entities, our SIM data provide evidence that SYP-1 can be loaded between the X sister chromatids (Figure 2, E–H). We propose that the X sister chromatids behave as homologs during the window when DSBs are induced to promote HR using the "sister" as a repair template (Figure 11). This configuration of the X chromosome may counteract the homolog bias mediated by the chromosome axis (Couteau *et al.* 2004). One prediction of such a model is that meiotic SCC is altered to enable sisters to interact as homologs. Consistent with this, the meiotic kleisins REC-8 and COH-3 have altered patterns of localization on the X in TZ when SYP-1 is loaded (Figure 3). Further, in contrast to autosome pairs, RAD-51 is disassembled on the X with apparently normal kinetics when all three meiotic kleisins are inactivated (Figure 4), suggesting that the majority of DSBs on the X can be repaired in the absence of meiotic kleisins. Finally, during the period when SYP-1 is loaded, sister chromatid association is not dependent on meiotic kleisins (Figure 4). This model also provides an explanation for why the SMC-5/6 complex, which has been suggested to mediate intersister recombination in the hermaphrodite germ line (Bickel *et al.* 2010), is not required for DSB repair on the X as monitored by RAD-51 disassembly as well as transmission through meiosis and chromosome fragmentation (Figure 5, Figure 6, and Figure S3). This is in contrast to delayed disassembly of RAD-51 on unpaired autosomes in *smc-6* mutants (Figure 5 and Figure S2), indicating that the X chromosome is unique in its lack of requirement for the SMC-5/6 complex.

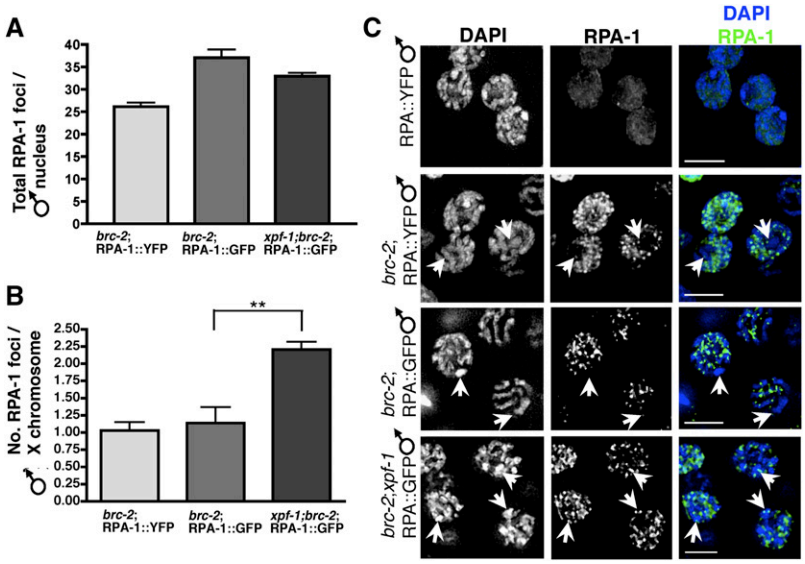

Figure 10 BRC-2 is dispensable for RPA removal on the male X. (A and B) Total and X chromosome-specific RPA-1 foci in *brc-2(tm1086)*; RPA-1::YFP (n = 71), *brc-2*; RPA-1::GFP, (n = 22) and *xpf-1*; *brc-2*; RPA-1::GFP (n = 103) male nuclei in late pachytene. In wild type (RPA-1::YFP, n = 48), very few RPA foci are observed (RPA-1 foci/X chromosome = 0.04167+/-0.02915). (C) Late pachytene nuclei corresponding to the strains in A and B showing RPA-1 foci (right column, green in merge) in nuclei counterstained with DAPI (blue). White arrowheads indicate the X chromosome, identified by absence of H3K4me2 (not shown) and morphology. Bars, 5 μm.

SC polymerization is dynamic, processive, and has a propensity to assemble on any available substrate (Voelkel-Meiman *et al.* 2012). What then removes SYP-1 specifically from the X chromosome at the onset of pachytene, well before it is disassembled from autosomes? SYP-1 localization parallels REC-8 localization, suggesting that the removal of SYP-1 follows the removal of REC-8 at the TZ/EP transition. However, it is unclear what removes REC-8 at the onset of pachytene only from the X (Figure 3). One possibility is that both SYP-1 and REC-8 are disassembled as the X chromosome condenses beginning in early pachytene. X chromatin condensation correlates with enrichment of repressive histone modifications (Kelly *et al.* 2002); however, even in the absence of the repressive histone mark H3K9me2, the X can be distinguished by its compact nature (Checchi and Engebrecht 2011), suggesting that multiple complexes are required for condensation and perhaps by extension SYP-1 and REC-8 removal from the X.

Just as the chromosomal basis of sex has evolved multiple times, it is also likely that the process by which meiosis has been altered to accommodate hemizygosity of sex chromosomes has evolved independently numerous times. Interestingly, in mouse spermatocytes, the SYP-1 equivalent SYCP1 is observed in patches along the non-PAR regions of the X and Y chromosomes (Page *et al.* 2006a), suggesting that central region components of the SC are loaded on regions of mammalian sex chromosomes that are neither synapsed nor homologous to each other. Further, in marsupials, the X and Y are completely nonhomologous yet are connected in meiotic prophase by a dense plate composed of the axial element SCP3 and the central region component SCP1 (Page *et al.* 2006b). Incorporation of SCP1 is homology independent and is proposed to be important for segregation of the sex chromosomes. Thus, association of central region components of the SC on nonhomologous regions of sex chromosomes may be a relatively general feature of hemizygous sex chromosomes during meiosis.

Regulation of X DSB processing and repair indicate a HR bias not directed toward crossing over

During meiosis, SPO-11-dependent DSBs are processed by a large set of proteins to promote repair by HR. Of critical importance is the CtIP/Sae2 homolog COM-1, which inhibits direct religation of DSBs by CKU-70/80, prior to RAD-51 filament formation (Lemmens *et al.* 2013). DSBs on all chromosomes of males, including the X, are subject to COM-1-dependent regulation as the numbers of both genome-wide and X-specific RAD-51 foci were significantly reduced in *com-1* mutants (Figure 7). This suggests that initial processing of DSBs is similar on autosomes and the X, and in both cases results in channeling repair through HR. Following nucleolytic degradation of the 5′ end, the resulting 3′ single-stranded DNA is immediately loaded by RPA-1, which is subsequently displaced by RAD-51 via BRC-2 (Martin *et al.* 2005). Interestingly, we observed similar number and size of RAD-51 foci on the X and each autosome pair (Figure 8D), suggesting that early processing events leading up to strand exchange are similar between the X and autosomes. However, COSA-1, a protein that marks sites of interhomolog crossovers (Yokoo *et al.* 2012), is not loaded on the X chromosome of males (Figure S4), indicating that DSBs are not designated to become COSA-1 marked crossovers. As crossover sites define bivalent asymmetry for reductional segregation (Nabeshima *et al.* 2005), and X sisters remain associated through meiosis I (Albertson and Thomson 1993; Shakes *et al.* 2009), it is likely that a crossover on the X would interfere with segregation at the first meiotic division. Taken together, these observations suggest that a step subsequent to strand exchange excludes X recombination sites from being designated as crossovers.

A number of recent studies have provided evidence that robust feedback mechanisms are in place during meiotic prophase to ensure regulated crossover formation (Carballo *et al.* 2013; Kauppi *et al.* 2013; Rosu *et al.* 2013; Stamper

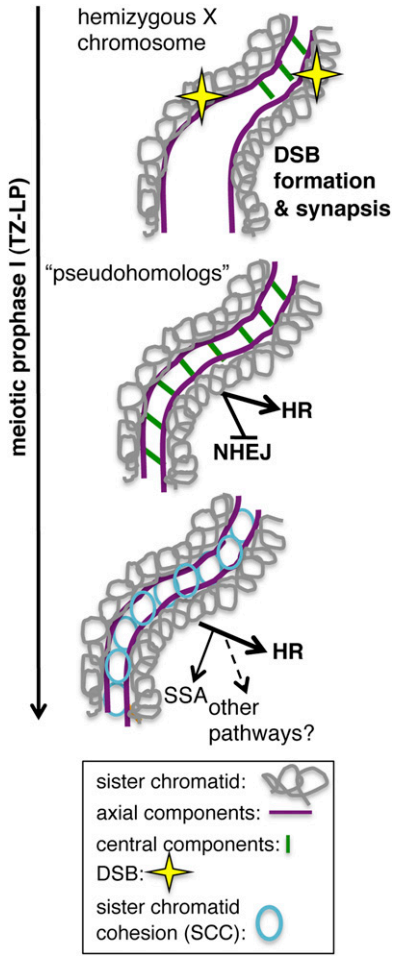

Figure 11 Model of X chromosome behavior during male meiosis. Early during prophase the X chromosome loads SYP-1 concomitant with RAD-51 assembly, driving repair of breaks through noncrossover homologous recombination (HR). As prophase proceeds, SYP-1 is disassembled and meiotic cohesins accumulate on the X. If HR repair is blocked as in *rad-54* or *brc-2* mutants, an XPF-1-dependent SSA pathway can be engaged on the X.

et al. 2013). In both yeast and mice, the ATM checkpoint protein plays a critical role in feedback regulation by inhibiting break formation; consequently, in the absence of ATM more DSBs are formed. Similarly, we found that in the *C. elegans* germ line, *atm-1* mutants have elevated RAD-51 foci throughout meiotic prophase in both hermaphrodites and males (Figure 7 and Figure S5). Work from the Dernburg and Villeneuve labs has revealed that failure to form a crossover intermediate, as in *rad-54* mutants, results in extension of the period of time in which breaks are formed (Rosu *et al.* 2013; Stamper *et al.* 2013). As *rad-54*; *atm-1(RNAi)* mutants have more RAD-51 foci than either of the single mutants (Figure 7 and Figure S5), we interpret this to mean that ATM-1 inhibits break formation independent of the crossover precursor signal that extends the time when breaks can be formed. Interestingly, we found that the X chromosome of males is not subject to this ATM-1 feedback regulation, suggesting that during processing, X breaks become differentiated from breaks on autosomes. These results are also consistent with our previous analyses of X DSBs not being detected by checkpoint machinery (Jaramillo-Lambert and Engebrecht 2010; Checchi and Engebrecht 2011). The interplay between checkpoint machinery, DSB processing and chromatin environment on the X is currently being investigated.

Prevalence of error-prone repair pathways in meiosis

Although we propose that noncrossover HR is the predominant mode of DSB repair on the X chromosome, inactivation of HR by mutation of either RAD-54 or BRC-2 does not block repair on the X to the same extent as on autosomes (Figure 8, Figure 9, and Figure 10). Repair of X DSBs is significantly impaired in the absence of either RAD-54 or BRC-2 and the structure-specific nuclease XPF-1. While recent studies have revealed a role for XPF-1 in crossover resolution, it is clear that XPF-1 plays additional roles in the germ line (Agostinho *et al.* 2013; O'Neil *et al.* 2013; Saito *et al.* 2013) and has been shown to function in SSA in somatic cells (Al-Minawi *et al.* 2008; Pontier and Tijsterman 2009). Genetic analysis in *C. elegans* revealed that in addition to the critical role BRC-2 plays in promoting RAD-51 filament formation, BRC-2 also functions independently of RAD-51 in DSB repair (Martin *et al.* 2005). As *C. elegans* does not have a Rad52 ortholog, it was suggested that BRC-2 mediates SSA. However, our results suggest that BRC-2 and XPF-1 define two genetically separable pathways for RAD-51-independent repair, and that DSB repair on the X can proceed in the absence of BRC-2 function. Thus, when HR is blocked subsequent to DSB resection as in *brc-2* or *rad-54* mutants, we propose that XPF-1-dependent SSA is the predominant pathway for DSB repair on the X chromosome of males (Figure 11).

Error-prone pathways such as NHEJ and SSA are believed to be the last resort for repair of DSBs in meiosis due to their propensity to cause mutations or chromosome abnormalities that could result in inviable progeny or be passed on to the next generation and lead to sterility. In the hermaphrodite germ line, NHEJ is engaged only at the very end of prophase after an extended period of time where HR is the predominant mode of repair (Colaiacovo *et al.* 2003; Hayashi *et al.* 2007). Release from the HR mode in hermaphrodites correlates with MAP kinase signaling (Hayashi *et al.* 2007). Males do not have MAP kinase signaling at this juncture of meiotic prophase (Lee *et al.* 2007), suggesting males regulate these processes differently. This is also supported by our observations that the overall kinetics of break repair are different in hermaphrodites and males. Nonetheless, our genetic and cytological analyses suggest that XPF-1 is only engaged to repair X DSBs and does not play a general role in break repair in the male germ line. One potential consequence of XPF-1-dependent repair would be a higher mutation rate on the X as compared to the autosomes, in lines maintained by outcrossing. Whether this is observed and

a consequence of the hermaphroditic life style of *C. elegans* or a more general property of sex chromosomes that contributes to their rapid evolution awaits future studies.

Acknowledgments

We thank A. Dernburg, J. Loidl, and A. Villeneuve for generously providing antibodies and the *Caenorhabditis* Genetic Center for strains. We also thank A. Severson for advice on using LacI-His_6-GFP, D. Cortez for advice on FISH, A. Villeneuve for helpful discussion, and E. Tapley and N. Andrews for critical reading of the manuscript. This work was supported by National Institutes of Health (NIH) GM103860 and the Agricultural Experimental Station California-Davis*MCB-7237-H (J.E.), NIH T32 CA10849 (P.M.C.), and NIH T32 GM0070377 (K.S.L.).

Literature Cited

Agostinho, A., B. Meier, R. Sonneville, M. Jagut, A. Woglar *et al.*, 2013 Combinatorial regulation of meiotic holliday junction resolution in *C. elegans* by HIM-6 (BLM) helicase, SLX-4, and the SLX-1, MUS-81 and XPF-1 nucleases. PLoS Genet. 9: e1003591.

Aguilera, A., and T. Garcia-Muse, 2013 Causes of genome instability. Annu. Rev. Genet. 47: 1–32.

Al-Minawi, A. Z., N. Saleh-Gohari, and T. Helleday, 2008 The ERCC1/XPF endonuclease is required for efficient single-strand annealing and gene conversion in mammalian cells. Nucleic Acids Res. 36: 1–9.

Albertson, D. G., and J. N. Thomson, 1993 Segregation of holocentric chromosomes at meiosis in the nematode, *Caenorhabditis elegans*. Chromosome Res. 1: 15–26.

Ashley, T., A. W. Plug, J. Xu, A. J. Solari, G. Reddy *et al.*, 1995 Dynamic changes in Rad51 distribution on chromatin during meiosis in male and female vertebrates. Chromosoma 104: 19–28.

Barchi, M., I. Roig, M. Di Giacomo, D. G. de Rooij, S. Keeney *et al.*, 2008 ATM promotes the obligate XY crossover and both crossover control and chromosome axis integrity on autosomes. PLoS Genet. 4: e1000076.

Bean, C. J., C. E. Schaner, and W. G. Kelly, 2004 Meiotic pairing and imprinted X chromatin assembly in *Caenorhabditis elegans*. Nat. Genet. 36: 100–105.

Bessler, J. B., E. C. Andersen, and A. M. Villeneuve, 2010 Differential localization and independent acquisition of the H3K9me2 and H3K9me3 chromatin modifications in the *Caenorhabditis elegans* adult germ line. PLoS Genet. 6: e1000830.

Bickel, J. S., L. Chen, J. Hayward, S. L. Yeap, A. E. Alkers *et al.*, 2010 Structural maintenance of chromosomes (SMC) proteins promote homolog-independent recombination repair in meiosis crucial for germ cell genomic stability. PLoS Genet. 6: e1001028.

Brenner, S., 1974 The genetics of *Caenorhabditis elegans*. Genetics 77: 71–94.

C. elegans Sequencing Consortium, 1998 Genome sequence of the nematode *C. elegans*: a platform for investigating biology. Science 282**:** 2012–2018.

Carballo, J. A., S. Panizza, M. E. Serrentino, A. L. Johnson, M. Geymonat *et al.*, 2013 Budding yeast ATM/ATR control meiotic double-strand break (DSB) levels by down-regulating Rec114, an essential component of the DSB-machinery. PLoS Genet. 9: e1003545.

Checchi, P. M., and J. Engebrecht, 2011 *Caenorhabditis elegans* histone methyltransferase MET-2 shields the male X chromosome from checkpoint machinery and mediates meiotic sex chromosome inactivation. PLoS Genet. 7: e1002267.

Clejan, I., J. Boerckel, and S. Ahmed, 2006 Developmental modulation of nonhomologous end joining in *Caenorhabditis elegans*. Genetics 173: 1301–1317.

Colaiacovo, M. P., A. J. MacQueen, E. Martinez-Perez, K. McDonald, A. Adamo *et al.*, 2003 Synaptonemal complex assembly in *C. elegans* is dispensable for loading strand-exchange proteins but critical for proper completion of recombination. Dev. Cell 5: 463–474.

Couteau, F., and M. Zetka, 2005 HTP-1 coordinates synaptonemal complex assembly with homolog alignment during meiosis in *C. elegans*. Genes Dev. 19: 2744–2756.

Couteau, F., K. Nabeshima, A. Villeneuve, and M. Zetka, 2004 A component of *C. elegans* meiotic chromosome axes at the interface of homolog alignment, synapsis, nuclear reorganization, and recombination. Curr. Biol. 14: 585–592.

Darby, R. A., and A. V. Hine, 2005 LacI-mediated sequence-specific affinity purification of plasmid DNA for therapeutic applications. FASEB J. 19: 801–803.

Dernburg, A. F., K. McDonald, G. Moulder, R. Barstead, M. Dresser *et al.*, 1998 Meiotic recombination in *C. elegans* initiates by a conserved mechanism and is dispensable for homologous chromosome synapsis. Cell 94: 387–398.

Fiorenza, M. T., A. Bevilacqua, S. Bevilacqua, and F. Mangia, 2001 Growing dictyate oocytes, but not early preimplantation embryos, of the mouse display high levels of DNA homologous recombination by single-strand annealing and lack DNA nonhomologous end joining. Dev. Biol. 233: 214–224.

Garcia, V., S. E. Phelps, S. Gray, and M. J. Neale, 2011 Bidirectional resection of DNA double-strand breaks by Mre11 and Exo1. Nature 479: 241–244.

Giroux, C. N., M. E. Dresser, and H. F. Tiano, 1989 Genetic control of chromosome synapsis in yeast meiosis. Genome 31: 88–94.

Goldfarb, T., and M. Lichten, 2010 Frequent and efficient use of the sister chromatid for DNA double-strand break repair during budding yeast meiosis. PLoS Biol. 8: e1000520.

Gonzalez-Serricchio, A. S., and P. W. Sternberg, 2006 Visualization of *C. elegans* transgenic arrays by GFP. BMC Genet. 7: 36.

Goodyer, W., S. Kaitna, F. Couteau, J. D. Ward, S. J. Boulton *et al.*, 2008 HTP-3 links DSB formation with homolog pairing and crossing over during *C. elegans* meiosis. Dev. Cell 14: 263–274.

Harper, N. C., R. Rillo, S. Jover-Gil, Z. J. Assaf, N. Bhalla *et al.*, 2011 Pairing centers recruit a Polo-like kinase to orchestrate meiotic chromosome dynamics in *C. elegans*. Dev. Cell 21: 934–947.

Hayashi, M., G. M. Chin, and A. M. Villeneuve, 2007 *C. elegans* germ cells switch between distinct modes of double-strand break repair during meiotic prophase progression. PLoS Genet. 3: e191.

Ho, H. C., and S. M. Burgess, 2011 Pch2 acts through Xrs2 and Tel1/ATM to modulate interhomolog bias and checkpoint function during meiosis. PLoS Genet. 7: e1002351.

Hodgkin, J., 1986 Sex determination in the nematode *C. elegans*: analysis of *tra-3* suppressors and characterization of *fem* genes. Genetics 114: 15–52.

Holloman, W. K., 2011 Unraveling the mechanism of BRCA2 in homologous recombination. Nat. Struct. Mol. Biol. 18: 748–754.

Hong, S., Y. Sung, M. Yu, M. Lee, N. Kleckner *et al.*, 2013 The logic and mechanism of homologous recombination partner choice. Mol. Cell 51: 440–453.

Jaramillo-Lambert, A., M. Ellefson, A. M. Villeneuve, and J. Engebrecht, 2007 Differential timing of S phases, X chromosome replication,

and meiotic prophase in the *C. elegans* germ line. Dev. Biol. 308: 206–221.

Jaramillo-Lambert, A., and J. Engebrecht, 2010 A single unpaired and transcriptionally silenced X chromosome locally precludes checkpoint signaling in the *Caenorhabditis elegans* germ line. Genetics 184: 613–628.

Jaramillo-Lambert, A., Y. Harigaya, J. Vitt, A. Villeneuve, and J. Engebrecht, 2010 Meiotic errors activate checkpoints that improve gamete quality without triggering apoptosis in male germ cells. Curr. Biol. 20: 2078–2089.

Joyce, E. F., A. Paul, K. E. Chen, N. Tanneti, and K. S. McKim, 2012 Multiple barriers to nonhomologous DNA end joining during meiosis in Drosophila. Genetics 191: 739–746.

Kamath, R. S., and J. Ahringer, 2003 Genome-wide RNAi screening in *Caenorhabditis elegans*. Methods 30: 313–321.

Kauppi, L., M. Barchi, F. Baudat, P. J. Romanienko, S. Keeney *et al.*, 2011 Distinct properties of the XY pseudoautosomal region crucial for male meiosis. Science 331: 916–920.

Kauppi, L., M. Barchi, J. Lange, F. Baudat, M. Jasin *et al.*, 2013 Numerical constraints and feedback control of double-strand breaks in mouse meiosis. Genes Dev. 27: 873–886.

Keeney, S., C. N. Giroux, and N. Kleckner, 1997 Meiosis-specific DNA double-strand breaks are catalyzed by Spo11, a member of a widely conserved protein family. Cell 88: 375–384.

Kelly, W. G., C. E. Schaner, A. F. Dernburg, M. H. Lee, S. K. Kim *et al.*, 2002 X-chromosome silencing in the germline of *C. elegans*. Development 129: 479–492.

Kim, K. P., B. M. Weiner, L. Zhang, A. Jordan, J. Dekker *et al.*, 2010 Sister cohesion and structural axis components mediate homolog bias of meiotic recombination. Cell 143: 924–937.

Lange, J., H. Skaletsky, S. K. van Daalen, S. L. Embry, C. M. Korver *et al.*, 2009 Isodicentric Y chromosomes and sex disorders as byproducts of homologous recombination that maintains palindromes. Cell 138: 855–869.

Lee, M. H., M. Ohmachi, S. Arur, S. Nayak, R. Francis *et al.*, 2007 Multiple functions and dynamic activation of MPK-1 extracellular signal-regulated kinase signaling in *Caenorhabditis elegans* germline development. Genetics 177: 2039–2062.

Lemmens, B. B., N. M. Johnson, and M. Tijsterman, 2013 COM-1 promotes homologous recombination during *Caenorhabditis elegans* meiosis by antagonizing Ku-mediated non-homologous end joining. PLoS Genet. 9: e1003276.

Liu, H., J. K. Jang, N. Kato, and K. S. McKim, 2002 mei-P22 encodes a chromosome-associated protein required for the initiation of meiotic recombination in *Drosophila melanogaster*. Genetics 162: 245–258.

MacQueen, A. J., M. P. Colaiacovo, K. McDonald, and A. M. Villeneuve, 2002 Synapsis-dependent and -independent mechanisms stabilize homolog pairing during meiotic prophase in *C. elegans*. Genes Dev. 16: 2428–2442.

Manfrini, N., I. Guerini, A. Citterio, G. Lucchini, and M. P. Longhese, 2010 Processing of meiotic DNA double strand breaks requires cyclin-dependent kinase and multiple nucleases. J. Biol. Chem. 285: 11628–11637.

Martin, J. S., N. Winkelmann, M. I. Petalcorin, M. J. McIlwraith, and S. J. Boulton, 2005 RAD-51-dependent and -independent roles of a *Caenorhabditis elegans* BRCA2-related protein during DNA double-strand break repair. Mol. Cell. Biol. 25: 3127–3139.

Martinez-Perez, E., and A. M. Villeneuve, 2005 HTP-1-dependent constraints coordinate homolog pairing and synapsis and promote chiasma formation during *C. elegans* meiosis. Genes Dev. 19: 2727–2743.

McKee, B. D., and M. A. Handel, 1993 Sex chromosomes, recombination, and chromatin conformation. Chromosoma 102: 71–80.

Mets, D. G., and B. J. Meyer, 2009 Condensins regulate meiotic DNA break distribution, thus crossover frequency, by controlling chromosome structure. Cell 139: 73–86.

Moens, P. B., D. J. Chen, Z. Shen, N. Kolas, M. Tarsounas *et al.*, 1997 Rad51 immunocytology in rat and mouse spermatocytes and oocytes. Chromosoma 106: 207–215.

Nabeshima, K., A. M. Villeneuve, and M. P. Colaiacovo, 2005 Crossing over is coupled to late meiotic prophase bivalent differentiation through asymmetric disassembly of the SC. J. Cell Biol. 168: 683–689.

Niu, H., L. Wan, B. Baumgartner, D. Schaefer, J. Loidl *et al.*, 2005 Partner choice during meiosis is regulated by Hop1-promoted dimerization of Mek1. Mol. Biol. Cell 16: 5804–5818.

Niu, H., L. Wan, V. Busygina, Y. Kwon, J. A. Allen *et al.*, 2009 Regulation of meiotic recombination via Mek1-mediated Rad54 phosphorylation. Mol. Cell 36: 393–404.

O'Neil, N. J., J. S. Martin, J. L. Youds, J. D. Ward, M. I. Petalcorin *et al.*, 2013 Joint molecule resolution requires the redundant activities of MUS-81 and XPF-1 during *Caenorhabditis elegans* meiosis. PLoS Genet. 9: e1003582.

Page, J., R. de la Fuente, R. Gomez, A. Calvente, A. Viera *et al.*, 2006a Sex chromosomes, synapsis, and cohesins: a complex affair. Chromosoma 115: 250–259.

Page, J., A. Viera, M. T. Parra, R. de la Fuente, J. A. Suja *et al.*, 2006b Involvement of synaptonemal complex proteins in sex chromosome segregation during marsupial male meiosis. PLoS Genet. 2: e136.

Pasierbek, P., M. Jantsch, M. Melcher, A. Schleiffer, D. Schweizer *et al.*, 2001 A *Caenorhabditis elegans* cohesion protein with functions in meiotic chromosome pairing and disjunction. Genes Dev. 15: 1349–1360.

Phillips, C. M., and A. F. Dernburg, 2006 A family of zinc-finger proteins is required for chromosome-specific pairing and synapsis during meiosis in *C. elegans*. Dev. Cell 11: 817–829.

Pontier, D. B., and M. Tijsterman, 2009 A robust network of double-strand break repair pathways governs genome integrity during *C. elegans* development. Curr. Biol. 19: 1384–1388.

Romanienko, P. J., and R. D. Camerini-Otero, 2000 The mouse Spo11 gene is required for meiotic chromosome synapsis. Mol. Cell 6: 975–987.

Rosu, S., K. A. Zawadzki, E. L. Stamper, D. E. Libuda, A. L. Reese *et al.*, 2013 The *C. elegans* DSB-2 protein reveals a regulatory network that controls competence for meiotic DSB formation and promotescrossover assurance. PLoS Genet. 9: e1003674.

Saito, T. T., J. L. Youds, S. J. Boulton, and M. P. Colaiacovo, 2009 *Caenorhabditis elegans* HIM-18/SLX-4 interacts with SLX-1 and XPF-1 and maintains genomic integrity in the germline by processing recombination intermediates. PLoS Genet. 5: e1000735.

Saito, T. T., D. Y. Lui, H. M. Kim, K. Meyer, and M. P. Colaiacovo, 2013 Interplay between structure-specific endonucleases for crossover control during *Caenorhabditis elegans* meiosis. PLoS Genet. 9: e1003586.

Schedl, T., and J. Kimble, 1988 *fog-2*, a germ-line-specific sex determination gene required for hermaphrodite spermatogenesis in *Caenorhabditis elegans*. Genetics 119: 43–61.

Schvarzstein, M., S. M. Wignall, and A. M. Villeneuve, 2010 Coordinating cohesion, co-orientation, and congression during meiosis: lessons from holocentric chromosomes. Genes Dev. 24: 219–228.

Sciurano, R. B., M. I. Rahn, M. I. Pigozzi, S. B. Olmedo, and A. J. Solari, 2006 An azoospermic man with a double-strand DNA break-processing deficiency in the spermatocyte nuclei: case report. Hum. Reprod. 21: 1194–1203.

Severson, A. F., L. Ling, V. van Zuylen, and B. J. Meyer, 2009 The axial element protein HTP-3 promotes cohesin loading and meiotic axis assembly in *C. elegans* to implement the meiotic program of chromosome segregation. Genes Dev. 23: 1763–1778.

Shakes, D. C., J. C. Wu, P. L. Sadler, K. Laprade, L. L. Moore *et al.*, 2009 Spermatogenesis-specific features of the meiotic program in *Caenorhabditis elegans*. PLoS Genet. 5: e1000611.

Shi, Q., E. Spriggs, L. L. Field, E. Ko, L. Barclay *et al.*, 2001 Single sperm typing demonstrates that reduced recombination is associated with the production of aneuploid 24,XY human sperm. Am. J. Med. Genet. 99: 34–38.

Shin, Y. H., M. M. McGuire, and A. Rajkovic, 2013 Mouse HORMAD1 is a meiosis I checkpoint protein that modulates DNA double- strand break repair during female meiosis. Biol. Reprod. 89: 29.

Smolikov, S., K. Schild-Prufert, and M. P. Colaiacovo, 2008 CRA-1 uncovers a double-strand break-dependent pathway promoting the assembly of central region proteins on chromosome axes during *C. elegans* meiosis. PLoS Genet. 4: e1000088.

Solinger, J. A., K. Kiianitsa, and W. D. Heyer, 2002 Rad54, a Swi2/Snf2-like recombinational repair protein, disassembles Rad51:dsDNA filaments. Mol. Cell 10: 1175–1188.

Sonneville, R., M. Querenet, A. Craig, A. Gartner, and J. J. Blow, 2012 The dynamics of replication licensing in live *Caenorhabditis elegans* embryos. J. Cell Biol. 196: 233–246.

Stamper, E. L., S. E. Rodenbusch, S. Rosu, J. Ahringer, A. M. Villeneuve *et al.*, 2013 Identification of DSB-1, a protein required for initiation of meiotic recombination in *Caenorhabditis elegans*, illuminates a crossover assurance checkpoint. PLoS Genet. 9: e1003679.

Stergiou, L., R. Eberhard, K. Doukoumetzidis, and M. O. Hengartner, 2011 NER and HR pathways act sequentially to promote UV-C-induced germ cell apoptosis in *Caenorhabditis elegans*. Cell Death Differ. 18: 897–906.

Terasawa, M., T. Ogawa, Y. Tsukamoto, and H. Ogawa, 2008 Sae2p phosphorylation is crucial for cooperation with Mre11p for resection of DNA double-strand break ends during meiotic recombination in *Saccharomyces cerevisiae*. Genes Genet. Syst. 83: 209–217.

Timmons, L., D. L. Court, and A. Fire, 2001 Ingestion of bacterially expressed dsRNAs can produce specific and potent genetic interference in *Caenorhabditis elegans*. Gene 263: 103–112.

Turner, J. M., 2007 Meiotic sex chromosome inactivation. Development 134: 1823–1831.

Tzur, Y. B., C. Egydio de Carvalho, S. Nadarajan, I. Van Bostelen, Y. Gu *et al.*, 2012 LAB-1 targets PP1 and restricts Aurora B kinase upon entrance into meiosis to promote sister chromatid cohesion. PLoS Biol. 10: e1001378.

van Attikum, H., and S. M. Gasser, 2009 Crosstalk between histone modifications during the DNA damage response. Trends Cell Biol. 19: 207–217.

Voelkel-Meiman, K., S. S. Moustafa, P. Lefrancois, A. M. Villeneuve, and A. J. MacQueen, 2012 Full-length synaptonemal complex grows continuously during meiotic prophase in budding yeast. PLoS Genet. 8: e1002993.

Woglar, A., A. Daryabeigi, A. Adamo, C. Habacher, T. Machacek *et al.*, 2013 Matefin/SUN-1 phosphorylation is part of a surveillance mechanism to coordinate chromosome synapsis and recombination with meiotic progression and chromosome movement. PLoS Genet. 9: e1003335.

Yan, R., and B. D. McKee, 2013 The cohesion protein SOLO associates with SMC1 and is required for synapsis, recombination, homolog bias and cohesion and pairing of centromeres in Drosophila meiosis. PLoS Genet. 9: e1003637.

Yin, Y., and S. Smolikove, 2013 Impaired resection of meiotic double-strand breaks channels repair to nonhomologous end joining in *Caenorhabditis elegans*. Mol. Cell. Biol. 33: 2732–2747.

Yokoo, R., K. A. Zawadzki, K. Nabeshima, M. Drake, S. Arur *et al.*, 2012 COSA-1 reveals robust homeostasis and separable licensing and reinforcement steps governing meiotic crossovers. Cell 149: 75–87.

Zakharyevich, K., Y. Ma, S. Tang, P. Y. Hwang, S. Boiteux *et al.*, 2010 Temporally and biochemically distinct activities of Exo1 during meiosis: double-strand break resection and resolution of double Holliday junctions. Mol. Cell 40: 1001–1015.

Zanetti, S., and A. Puoti, 2013 Sex determination in the *Caenorhabditis elegans* germline. Adv. Exp. Med. Biol. 757: 41–69.

Zhang, W., N. Miley, M. S. Zastrow, A. J. MacQueen, A. Sato *et al.*, 2012 HAL-2 promotes homologous pairing during *Caenorhabditis elegans* meiosis by antagonizing inhibitory effects of synaptonemal complex precursors. PLoS Genet. 8: e1002880.

Communicating editor: M. C. Zetka

GENETICS

Supporting Information
http://www.genetics.org/lookup/suppl/doi:10.1534/genetics.114.164152/-/DC1

Pseudosynapsis and Decreased Stringency of Meiotic Repair Pathway Choice on the Hemizygous Sex Chromosome of *Caenorhabditis elegans* Males

Paula M. Checchi, Katherine S. Lawrence, Mike V. Van, Braden J. Larson, and JoAnne Engebrecht

DOI: 10.1534/genetics.114.164152

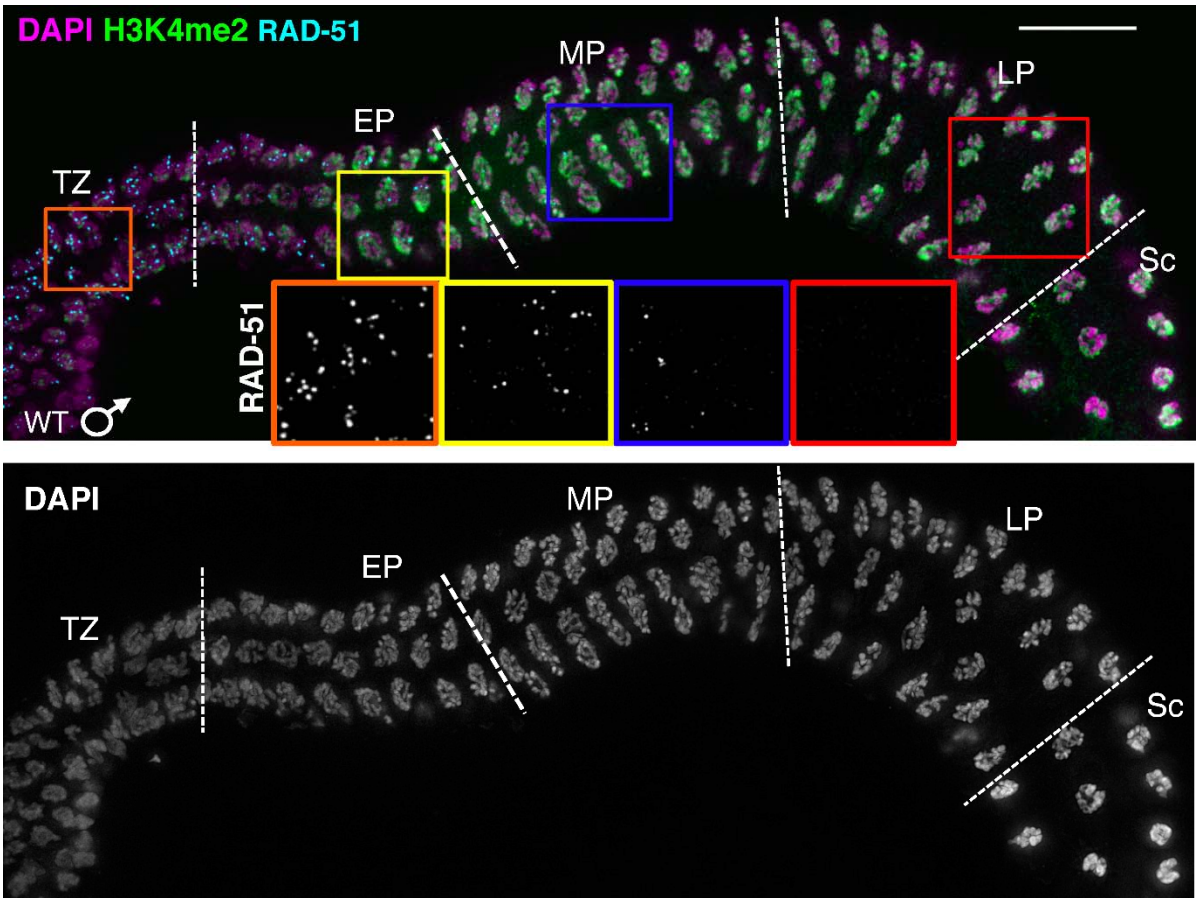

Figure S1 Spatial and temporal distribution of RAD-51 foci during prophase of male meiosis. (A) Section of male germ line corresponding to prophase I stained with RAD-51 (cyan, insets), H3K4me2 (green) and counterstained with DAPI (magenta). Bottom row shows DAPI morphology, which was used with absence of H3K4me2 (green) to identify the X chromosome throughout these stages. Dashed lines indicate substages between transition zone (TZ, orange), early pachytene (EP, yellow), mid pachytene (MP, blue), late pachytene (LP, red), and spermatocytes (Sc, diplotene-diakinesis). Beginning and end of TZ were determined by DAPI morphology, and pachytene substages were divided by counting total rows of nuclei in this region and dividing by three. Insets compare RAD-51 abundance from TZ to LP. Scale bar = 15μm.

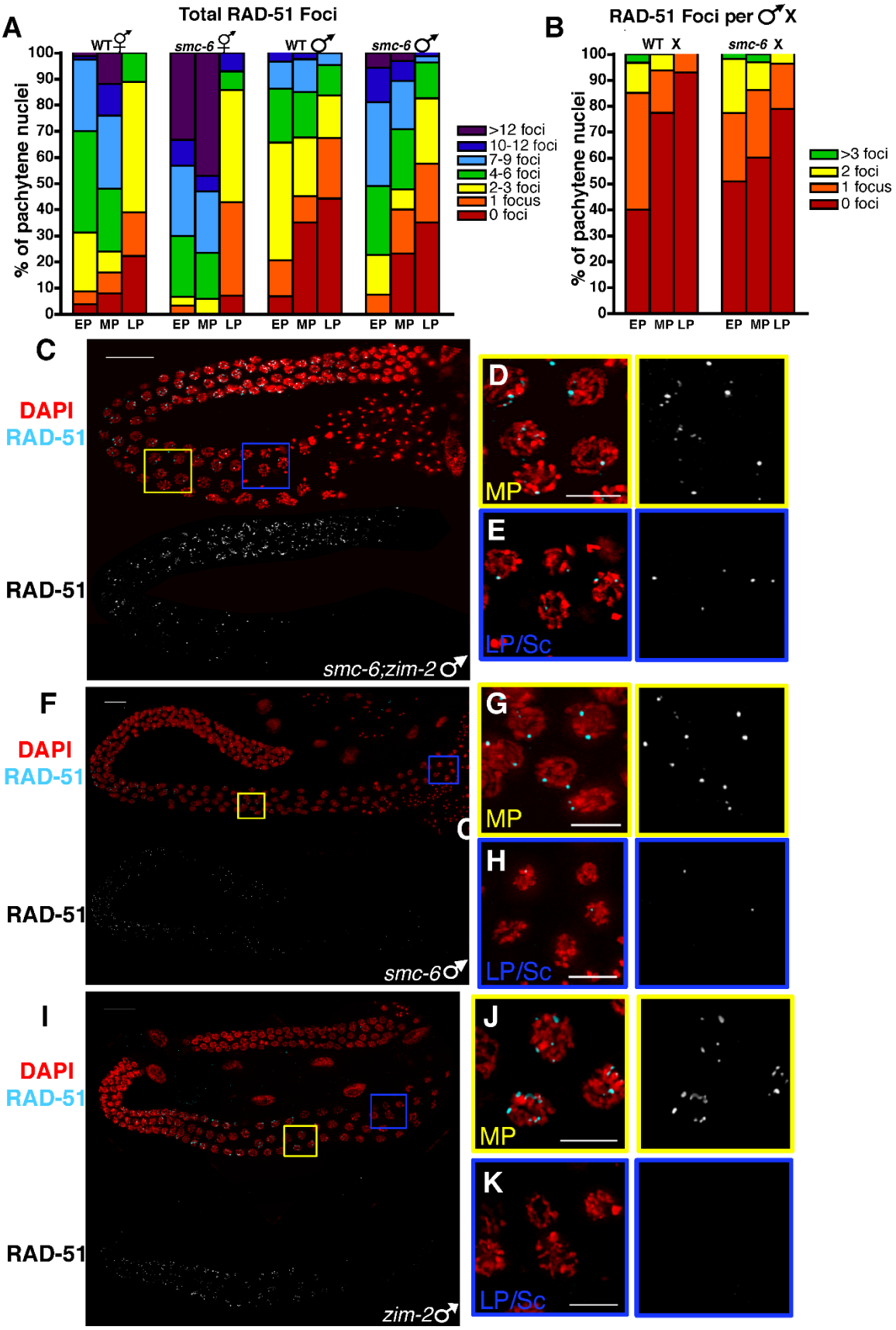
A
Total RAD-51 Foci
WT ♀
smc-6 ♀
WT ♂
smc-6 ♂
% of pachytene nuclei
EP MP LP
>12 foci
10-12 foci
7-9 foci
4-6 foci
2-3 foci
1 focus
0 foci
B
RAD-51 Foci per ♂X
WT X
smc-6 X
>3 foci
2 foci
1 focus
0 foci
C
DAPI
RAD-51
RAD-51
smc-6;zim-2 ♂
D
MP
E
LP/Sc
F
DAPI
RAD-51
RAD-51
smc-6 ♂
G
MP
H
LP/Sc
I
DAPI
RAD-51
RAD-51
zim-2 ♂
J
MP
K
LP/Sc

Figure S2 In the absence of SMC-6, RAD-51 disassembly is compromised on paired and unpaired autosomes but not the male X. (A-B) Comparison of total (A) and X-specific (B) RAD-51 in wild-type and *smc-6* germ lines throughout pachytene. (See also Figure 5.) (C-K) Whole-mount germ lines stained with RAD-51 (cyan) and counterstained with DAPI (red). Yellow boxes (D, G, J) indicate regions from mid pachytene (MP) and blue boxes (E, H, K) are LP/Sc. In *smc-6;zim-2* male germ lines (C-E), RAD-51 persists through late pachytene (LP) and is detected on spermatocytes (Sc) nuclei. In *smc-6* (F-H) and *zim-2* (I-K) germ lines, RAD-51 persists through MP, but fewer foci remain by LP/Sc. (C, F, I) Scale bars = 15μm; (D, E, G, H, J,K) Scale bars = 5μm.

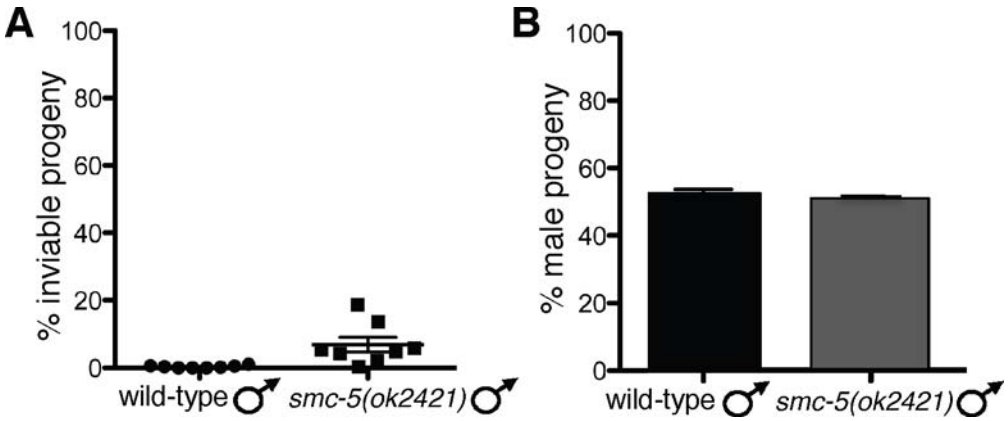

Figure S3 Fertilization by *smc-5* male sperm results in progeny inviability but does not affect X chromosome transmission. (A) Percent inviable progeny were determined from eight independent crosses of wild-type or *smc-5(ok2421)* males to *fog-2(q71)* females. (B) Percent male progeny were determined from ten independent crosses of wild-type (black) or *smc-5(ok2421)* (grey) males to *fog-2(q71)* females. No significant differences were observed using the Student t-test.

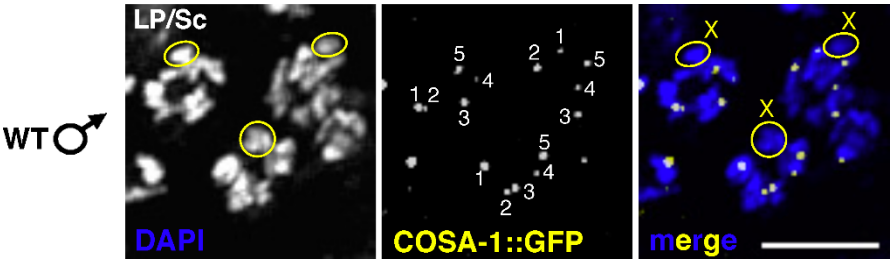

Figure S4 COSA-1-dependent crossovers are not observed on the X chromosome of males. Wild-type late pachytene (LP) male nucleus expressing COSA-1::GFP (sites of crossovers, yellow in merge) and counterstained with DAPI (red). Yellow circles indicate the X chromosome. White numbers denote individual COSA-1 foci detected (five per male nucleus). Scale bar = 5μm.

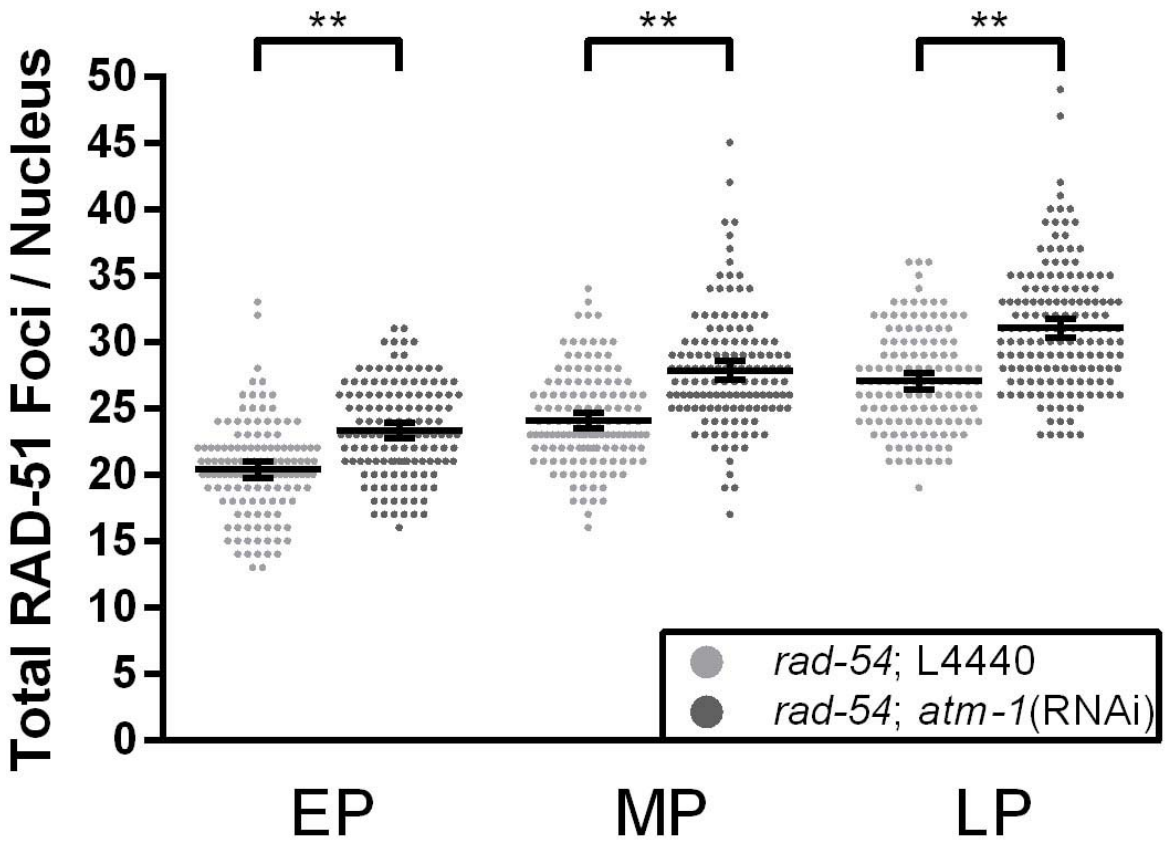

Figure S5 ATM-1 negatively regulates DSB formation. Scatter plot of total RAD-51 foci/nucleus in *rad-54(ok615);him-8(me4)* and *rad-54;him-8(me4);atm-1*(RNAi) male gonads. *rad-54;him-8;atm-1*(RNAi) male gonads contain more RAD-51 foci per nucleus than *rad-54;him-8* male gonads fed empty L4440 vector. Nuclei were scored as described in Figure S1. Total nuclei scored: *rad-54;him-8*: EP n=130, MP n=135, LP n=134. *rad-51;him-8*;*atm-1*(RNAi): EP n=136, MP n=138, LP n=157. Horizontal black lines correspond to the means of each data set and error bars represent the 95% confidence interval of the mean. Data were analyzed using a two-tailed Mann-Whitney test. ** = $p<0.0001$.

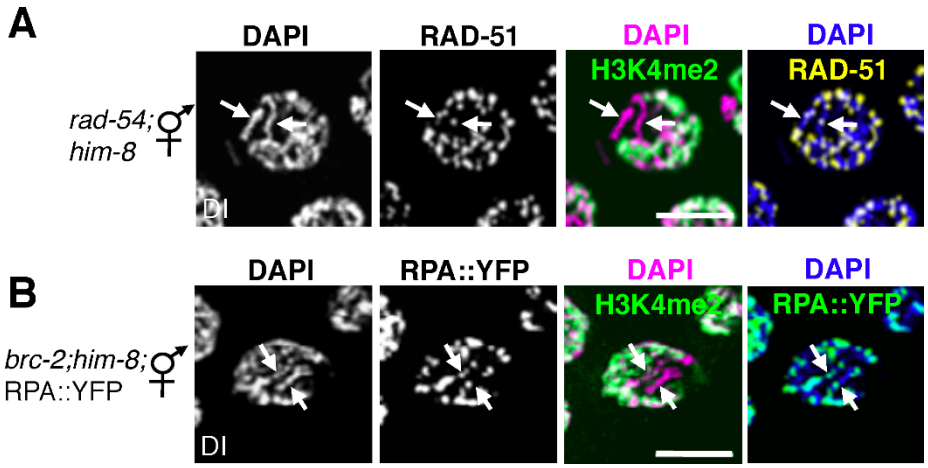

Figure S6 Asynapsed X chromosomes are defective in DSB repair. Diplotene (DI) stage nuclei from (A) *rad-54(ok615);him-8(me4)* and (B) *brc-2(tm1086);him-8(me4)* hermaphrodite germ lines possess a pair of asynapsed X chromosomes, indicated by white arrows and absence of H3K4me2 staining (green, left panels). (A) RAD-51 (yellow in merge) and (B) RPA::YFP (green in merge) persist on all chromosomes. Scale bars = 5 μM.

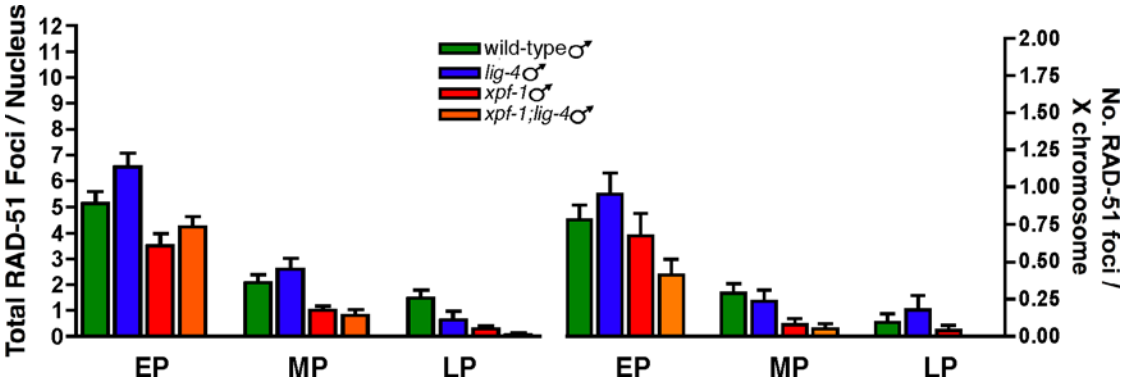

Figure S7 RAD-51 removal on the X chromosome is unaffected in SSA and NHEJ mutants competent for HR. Comparison of total RAD-51 foci (left) and X chromosome-specific RAD-51 (right) in wild-type (green, n=183), *lig-4* (blue, n=90), *xpf-1* (red, n=97), and *xpf-1;lig-4;him-8(me4)* (orange, n=157) male pachytene nuclei. Error bars = S.E.M. Total RAD-51 foci per nucleus: EP: wild-type (av=5.15+/-0.43), *lig-4* (av=6.54+/-0.54), *xpf-1* (av=3.52+/-0.47), *xpf-1;lig-4;him-8(me4)* (av=4.24+/-0.40); MP: wild type (av=2.09+/-0.31), *lig-4* (av=2.60+/-0.43), *xpf-1* (av=1.00+/-0.17), *xpf-1;lig-4;him-8(me4)* (av=0.82+/-0.22); LP: wild type (av=1.49+/-0.29), *lig-4* (av=0.65+/-0.32), *xpf-1* (av=0.30+/-0.13), *xpf-1;lig-4;him-8(me4)* (av=0.08+/-0.40). RAD-51 foci per X chromosome: EP: wild type (av=0.78+/-0.10), *lig-4* (av=0.95+/-0.14), *xpf-1* (av=0.68+/-0.15), *xpf-1;lig-4;him-8(me4)* (av=0.41+/-0.11); MP: wild-type (av=0.29+/-0.06), *lig-4* (av=0.23+/-0.08), *xpf-1* (av=0.08+/-0.04), *xpf-1;lig-4;him-8(me4)* (av=0.05+/-0.04); LP: wild type (av=0.09+/-0.06), *lig-4* (av=0.18+/-0.10), *xpf-1* (av=0.04+/-0.04), *xpf-1;lig-4;him-8(me4)* (av=0).